

Structure and kinetic properties of human D-aspartate oxidase, the enzyme controlling D-aspartate levels in brain

Gianluca Molla¹, Antonio Chaves-Sanjuan², Antonio Savinelli¹, Marco Nardini^{2*}, Loredano Pollegioni^{1*}

¹Dipartimento di Biotecnologie e Scienze della Vita, Università degli studi dell'Insubria, via J.H. Dunant 3, 21100 Varese, Italy. ²Dipartimento di Bioscienze, Università degli studi di Milano, via Celoria 26, 20133, Milano, Italy.

These authors contributed equally: Gianluca Molla, Antonio Chaves-Sanjuan and Antonio Savinelli.

*Correspondence and request for materials should be addressed to: Marco Nardini, Dipartimento di Bioscienze, Università degli studi di Milano, via Celoria 26, 20133, Milano, Italy, +390250314893 (marco.nardini@unimi.it) or to Loredano Pollegioni, Dipartimento di Biotecnologie e Scienze della Vita, Università degli studi dell'Insubria, via J.H. Dunant 3, 21100 Varese, Italy, +390332421506 (loredano.pollegioni@uninsubria.it)

Short title: Human D-aspartate oxidase

ABBREVIATIONS: AMPA, α -amino-3-hydroxy-5-methylisoxazole-4-propionic acid hydrate; 5-An, 5-aminonicotinic acid; CBIO, 6-chloro-1,2-benzisoxazol-3(2H)-one; DAAO, D-amino acid oxidase; DASPO or DDO, D-aspartate oxidase; DPPD, pyrido[2,3-b]pyrazine-2,3(1H,4H)-dione; hDAAO, human D-amino acid oxidase; hDASPO, human D-aspartate oxidase; MT, meso-tartrate; NAC, N-acetyl L-cysteine; NMDAR, N-methyl-D-aspartate receptor; OPA, *o*-phthaldialdehyde; RgDAAO, D-amino acid oxidase from *Rhodotorula gracilis*; OA, oxaloacetate; IAsp, iminoaspartate

ABSTRACT: D-Amino acids are the “wrong” enantiomers of amino acids: they are not used in proteins synthesis but evolved selected functions. On this side, D-aspartate plays several significant roles in mammals, especially as an agonist of N-methyl-D-aspartate receptors (NMDAR), and is involved in relevant diseases, such as schizophrenia and Alzheimer’s disease. *In vivo* modulation of D-aspartate levels represents an intriguing task to cope with such pathological states. As little is known about D-aspartate synthesis, the only option for modulating the levels is *via* degradation, which is due to the flavoenzyme D-aspartate oxidase (DASPO). Here we present the first three-dimensional structure of a DASPO enzyme (from human) which belongs to the D-amino acid oxidase family. Notably, human DASPO differs from human D-amino acid oxidase (attributed to D-serine degradation, the main coagonist of N-methyl-D-aspartate receptors) showing peculiar structural features (a specific active site charge distribution), oligomeric state and kinetic mechanism, and a higher FAD affinity and activity. These results provide useful insights into the structure-function relationships of human DASPO: modulating its activity represents now a feasible novel therapeutic target.

KEYWORDS: D-aspartate; D-aspartate oxidase; NMDA receptor; flavoprotein; structure-function relationships

In recent years, a number of studies focused on the physiological role of the “wrong” enantiomer of amino acids, namely, the D-amino acids, starting from simple bacteria up to humans (1-3). In mammals, D-serine (D-Ser) and D-aspartate (D-Asp) have attracted interest owing to their involvement in important physiological processes and pathological states (4-6). The metabolism of D-Ser in mammalian brain has been established (7,8), providing deep insight into the molecular mechanisms underlying relevant physiological processes (such as N-methyl-D-aspartate receptor (NMDAR)-mediated neurotransmission and brain functions such as learning and memory) and generating the opportunity to develop novel therapeutic approaches. However, this information is lacking for D-Asp, which is present in various mammalian tissues (9,10). In endocrine glands D-Asp levels rise during postnatal and adult developmental phases and correlate with the synthesis of different hormones in rodents as well as to the synthesis and release of melatonin (4, 11). Notably, the temporal occurrence of D-Asp in the brain, where it is mainly present in neurons (12,13), is the opposite: levels are highest during the embryonic stage and in the first days of life and are greatly reduced later on (14,15).

Whereas the synthetic pathway of D-Asp in mammals is still under debate - the presence of a specific racemase is still questioned, see (16) - it is catabolized by the oxidative deamination reaction catalyzed by the peroxisomal (17) flavoenzyme D-aspartate oxidase (DASPO or DDO, EC 1.4.3.1) to yield oxaloacetate, ammonia, and hydrogen peroxide. The decrease in brain D-Asp levels during the postnatal phase is due to the progressive expression of DASPO (15): in the adult brain D-Asp is localized inversely to DASPO (12).

D-Asp features many of the signatures of a classical neurotransmitter, for a review see (5). Owing to a relatively high affinity, D-Asp acts as an agonist on postsynaptic NMDAR (18). Indeed, it also stimulates mGlu5 receptors (metabotropic glutamate receptor 5) in neonate rat hippocampal and cortical slices (19) and presynaptic AMPA (α -amino-3-hydroxy-5-methylisoxazole-4-propionic acid hydrate), mGlu5, and NMDA receptors (20). D-Asp is able to rescue the age-related synaptic plasticity deterioration observed at the hippocampus in mice, likely counteracting the decrease in NMDAR signalling observed during aging (15). NMDAR hypofunction has been related to various brain disorders, such as schizophrenia, where a lower concentration of D-Asp in prefrontal cortex and striatum has been reported (21). Notably, adult mice with a DASPO gene knockout ($Ddo^{-/-}$) show increased D-Asp concentrations and possess enhanced NMDAR-dependent long-term potentiation in the CA1 area of the hippocampus (15,22), which has been considered as a neural mechanism for the storage of spatial information. Young $Ddo^{-/-}$ mice (4-5 months old) show improved spatial memory and cognitive ability, while a worsening of learning and memory abilities is observed in the same animals at 13-14 months of age (15). Concerning Alzheimer’s disease, D-Asp influences the process leading to A β 40 and A β 42 aggregation (23). Furthermore, chronic administration of D-Asp during remyelination had beneficial effects on oligodendrocyte lineage cells and improved motor coordination,

accelerated myelin recovery, and increased the amount of small-diameter myelinated axons acting on both NMDA and AMPA receptors (24).

As little is known about the synthetic side of D-Asp, the only option to modulate D-Asp levels in the brain is *via* degradation. The human *DDO* gene encodes for two mRNA forms generated by alternative splicing (25): *DDO-1* encodes a protein of 341 amino acids in length while *DDO-2* generates a truncated protein of 282 residues (probably an inactive variant). Full-length human DASPO (hDASPO) was overexpressed in *E. coli* cells: it contains one molecule of non-covalently bound FAD per 39 kDa protein monomer, is mainly active on D-Asp and NMDA, is stable up to 50 °C and in 8-11 pH range and its activity is not affected by metal ions or nucleotides as well as by L-Asp or L-Glu (25, 26). hDASPO is significantly more active on D-Asp than the corresponding rat and mouse counterparts (26, 27). So far, efficient inhibitors of hDASPO have not been identified: the best tested inhibitor is 5-aminonicotinic acid (5-An), whose K_i is only 3.8 μ M (27, 28). Recently, the R216Q and S308N hDASPO variants (substitutions corresponding to known single nucleotide polymorphisms present in the NCBI database) were characterized: the R216Q substitution significantly affected the apparent k_{cat} and K_m values for D-Asp and resulted in the ability to oxidize D-Ala (29). Indeed, compared to rat tumor GH₃ cells transiently expressing the wild-type hDASPO, the cellular level of D-Asp was affected to a minor extent by the expression of these two variant enzymes.

By combining X-ray crystallography with the investigation of steady state and pre-steady state kinetics, substrate preference, and interaction with classical inhibitors of amino acid oxidases and with the FAD cofactor, we gained deep insight into the structure-function relationships in hDASPO. The results highlight peculiar features of hDASPO relevant for controlling D-Asp cellular levels and have now paved the way for the challenge to rationally design inhibitors that could reduce D-Asp catabolism and potentially serve as novel antipsychotic drugs.

MATERIALS AND METHODS

Protein expression and purification

The synthetic cDNA coding for hDASPO was designed from the nucleotide sequence reported in GenBank® (accession number NM_003649). Codon optimization for expression in *E. coli* was performed according to the Codon Usage Database (<http://www.kazusa.or.jp/codon/>) by eliminating rare codons, i.e., codons used with a < 10% frequency for coding a given amino acid. Synthetic cDNA (GenBank accession number MK224818) was produced by GeneArt®. The cDNA molecule coding for hDASPO was cloned into a custom variant of pET11 expression vector (Novagen) possessing a sequence coding for a 6xHis upstream of the multiple cloning site. hDASPO was cloned between the *NheI* and *BamHI* restriction sites, producing the pET11-His-hDASPO plasmid coding for a N-terminal 6XHis-tagged recombinant protein. H54A and R237A hDASPO variants were

generated by site-directed mutagenesis using the QuikChange Lightning Site-Directed Mutagenesis kit (Agilent) as detailed in Supplementary Data 1.

For protein expression, pET11-His-hDASPO plasmid was transferred into *E. coli* BL21(DE3) LOBSTR host cells (Novagen). Starter cultures were prepared from a single colony of *E. coli* cells carrying the recombinant plasmid and growing at 37 °C on LB broth medium (10 g/L bacto tryptone, 5 g/L yeast extract and 5 g/L NaCl) to which the antibiotic ampicillin (100 µg/mL final concentration) was added. For protein purification, 2 L baffled flasks containing 500 mL of LB medium were inoculated with the starter culture (initial OD_{600nm} of 0.1) and grown at 37 °C under shaking (220 rpm) until a OD_{600nm} of 0.5 was reached. Protein expression was induced by adding 0.01 mM IPTG (final concentration); then, the incubation temperature was lowered to 30 °C. Cells were harvested 18 h after adding IPTG by centrifugation at 8000 g for 10 min at 4 °C. Cells were lysed by sonication (10 cycles of 25 s each, with 60-s intervals on ice) in 50 mM potassium phosphate (pH 8.0), 200 µM FAD, 1 mM PMSF, 5 mM 2-mercaptoethanol, 5 mM K/Na tartrate, 5% (v/v) glycerol, and 10 µg/mL DNase I. Cell lysates were centrifuged at 39000 g for 1 h at 4 °C. The crude extract was loaded on a HiTrap chelating column (GE Healthcare) preloaded with Ni²⁺ and equilibrated in 50 mM sodium pyrophosphate (pH 7.2), 1 M NaCl, 10 µM FAD, 5% (v/v) glycerol, and 5 mM K/Na tartrate. The bound protein was eluted from the column using 50 mM sodium pyrophosphate (pH 7.2), 0.25 M imidazole, 10 µM FAD, 10% (v/v) glycerol, and 5 mM K/Na tartrate. The purified protein was then transferred to storage buffer (20 mM Tris-HCl and 10% (v/v) glycerol, pH 8.0) by dialysis.

The apoprotein form of hDASPO was prepared by dialysis against halide anions and a mild denaturant at physiological pH, a procedure used to weaken the binding of FAD with the apoprotein moiety (30). In details, the enzyme was dialyzed at 4 °C against 20 mM TrisHCl, pH 8.0, 5 mM 2-mercaptoethanol, 10% glycerol, 1 M urea and: 1.5 M KBr for 8 hours, 2 M KBr for 16 hours, 2.5 M KBr for 8 hours and 3 M KBr for 16 hours. The caothropic salt (KBr) and the denaturing agent (urea) were eliminated by dialysis against 20 mM TrisHCl, pH 8.0, 5 mM 2-mercaptoethanol, 10% glycerol containing: 2 M KBr and 0.5 M urea for 4 hours, 1 M KBr and 0.25 M urea for 4 hours and no KBr and urea for 16 hours. The apoprotein recovery was 85%.

Spectroscopy and structural analysis

Absorbance data were recorded at 15 °C in 20 mM Tris-HCl, pH 8.0, 10% glycerol and 5 mM 2-mercaptoethanol. Dissociation constants for ligands were determined spectrophotometrically by adding small volumes (1–10 µL) of concentrated stock solutions to samples containing 1 mL of ~10 µM enzyme, at 15 °C. The change in absorbance at 494, 488, 501, 501, 502, 550, and 497 nm were used for L-(+)-tartrate, meso-tartrate, 6-chloro-1,2-benzisoxazol-3(2H)-one (CBIO), 5-aminonicotinic acid, pyrido[2,3-b]pyrazine-2,3(1H,4H)-dione (DPPD), anthranilate, and benzoate, respectively. Photoreduction experiments were carried

out at 4 °C using an anaerobic cuvette containing ~11 μM enzyme, 5 mM EDTA, and 60 nM deazaflavin (31). The solution was photoreduced with a 250-W lamp and the progress of the reaction was followed spectrophotometrically. All fluorescence measurements were performed at 15 °C and at 1 μM protein concentration in 20 mM Tris–HCl, 10% glycerol, and 5 mM 2-mercaptoethanol, pH 8.0. The binding constant for the cofactor was determined by titrating 1 μM hDASPO apoprotein with increasing amounts of FAD and following the quenching of the protein fluorescence at 341 nm.

Circular dichroism (CD) spectra were recorded using protein samples at 0.1 or 0.4 mg/mL for far-UV or near-UV measurements, respectively, in 20 mM potassium phosphate, 10% glycerol (v/v), and 150 mM NaCl at 15 °C. Temperature ramp experiments were carried out following the change in CD signal at 220 nm using a Peltier thermostatic system, from 20 to 100 °C (temperature ramp of 0.5 °C/min) (32).

The oligomeric state of hDASPO was determined by gel-permeation chromatography on a Superdex 200 (Amersham Biosciences) column using 20 mM Tris–HCl, pH 8.5, 150 mM NaCl, 5% glycerol, 5 mM 2-mercaptoethanol, and 40 μM FAD as elution buffer.

Kinetic measurements

The apparent kinetic parameters on different amino acids as substrate were determined in 100 mM disodium pyrophosphate buffer, pH 8.3, containing 40 μM FAD, at 25 °C and air saturation, measuring the oxygen consumption with an Hansatech oxygen electrode (31).

The rapid reaction measurements and the turnover experiments were performed in 100 mM disodium pyrophosphate buffer, pH 8.3, containing 1% glycerol, at 25 °C in a stopped-flow Bio-Logic SFM-300 spectrophotometer equipped with a J&M diode array detector (31). Enzyme monitored turnover data were analyzed according to the method described by (33). For reductive and oxidative half-reaction experiments, the stopped-flow instrument was made anaerobic by overnight equilibration with a sodium dithionite solution and then was rinsed with argon-equilibrated buffer. To eliminate oxygen residues, 2 mM D-alanine, 0.5 μM RgDAAO (D-amino acid oxidase from *Rhodotorula gracilis*) and 10 μg/μL catalase (added to eliminate H₂O₂ produced by RgDAAO reaction during O₂-depletion) was added to the enzyme before the mixing with D-Asp.

For the oxidative half-reaction experiments, the enzyme (15-25 μM) was first reduced with a 4-fold molar excess of D-Asp under anaerobic conditions. Solutions were made anaerobic in tonometers by 10 cycles of evacuation and equilibration with oxygen-purged argon, and substrate solutions were made anaerobic by bubbling with argon for at least 10 min in glass syringes (31). In selected experiments, in order to eliminate residual oxygen, the enzyme solution containing 2 mM D-Ala and 10 μg/μL catalase was mixed with 1 μM RgDAAO after the anaerobiosis (see above). For reoxidation experiments, different oxygen concentrations in

the reoxidation mixture were obtained by equilibrating the buffer solutions for ten minutes with commercially available N₂/O₂ mixtures (97.5:2.5, 90:10, 75:25, and 50:50, v/v), or with pure O₂.

Reaction rates were calculated by extracting traces at individual wavelengths (455 and 530 nm) and fitting them to a sum of exponentials equation using the program Biokine32 (Bio-Logic).

Crystallization, data collection, structure determination, and refinement

Extensive preliminary crystallization trials on the native hDASPO were not successful, often leading to amorphous precipitation. A general low solubility problem was also noted in solution during protein concentration. Therefore, we decided to check whether mutations on the nine Cys residues present in the hDASPO sequence could help solubility (by preventing interchain disulfide bridge formation) and crystallization. We first generated a 3D model using the I-TASSER (<http://zhanglab.ccmb.med.umich.edu/I-TASSER/>) and SwissModel (<http://swissmodel.expasy.org/>) servers with hDAAO as template (PDB 3G3E, 39% sequence identity). The conservation analysis by the ConSurf server (<http://consurf.tau.ac.il>) shows that among the nine Cys residues present in hDASPO, five are not conserved in hDAAO (namely, Cys29, Cys141, Cys143, Cys269, and Cys328) and two of these are not conserved in pig DASPO (Cys141 and Cys143), which has been crystallized in the past (34). Only Cys182 and Cys258 are conserved in all the hDASPO homologues and predicted to be not solvent exposed by our hDASPO model. Based on these analyses, Cys at positions 29, 269, and 328 (on the protein surface) and 141 and 143 (not conserved in crystallized hDAAO and pig DASPO) were selected for mutagenesis. Details regarding production and characterization of the variants are reported in Supplementary Data 1.

The hDASPO C141Y/C143G variant, which reproduces the pig DASPO amino acid pair (see below), was crystallized at 18 mg/mL in the presence of 60 μM FAD. Rod-shaped yellow crystals grew by dehydration of 0.2 μL drops supplemented with 5-50 mM NaCl after two weeks. Crystals were cryoprotected using a 20 mM Tris-HCl, pH 8.0, and 20% glycerol solution, frozen in liquid nitrogen, and tested at the Diamond light source (i04 beamline). A data set was reduced using XDS (35) and anisotropically truncated and scaled with STARANISO (36). The structure was solved by molecular replacement using the coordinates of hDAAO as a search model. Iterative cycles of model building with COOT (37) and refinement with PHENIX (38) were carried out to produce the final model. Stereochemical parameters of the final model was checked with MOLPROBITY (39). Data processing and refinement statistics are shown in Supplementary Table 1. Atomic coordinates and structure factors have been deposited at the Protein Data Bank with the accession code 6RKF.

Molecular docking

Molecular docking analysis was performed using the software Autodock Vina (40). The ligands were docked to the receptor hDASPO (chain A of the crystal structure) with flexible residues (His54, Arg216, Tyr223, Arg237, Arg278, Ser308). Ligands were prepared with the software Avogadro V1.2.0 (41). The search grid size was $25 \times 25 \times 25 \text{ \AA}$ centered on the position occupied by the glycerol ligand of the crystal structure.

RESULTS

Biochemical properties of hDASPO

Recombinant hDASPO (*DDO-1* isoform) was purified from the crude extract of *E. coli* BL21(DE3) LOBSTR cells bearing the pET11-His-hDASPO plasmid, grown under optimized conditions, see Methods. By using a single chromatographic step on a HiTrap chelating column we could purify $\sim 30 \text{ mg}$ of hDASPO/L of fermentation broth (a figure 10-fold higher than those previously reported, $\sim 2\text{-}3 \text{ mg/L}$) (25,26,28) with a purity $\sim 94\%$ as estimated by analysis by ImageJ software (see Supplementary Fig. 1 and Supplementary Data 1 for details about protein expression).

Recombinant hDASPO is highly specific for D-Asp and its derivative NMDA. It shows a lower activity on D-Glu and D-Asn (12.8% and 9.5% vs D-Asp, respectively) and also oxidizes D-His and D-Pro ($\sim 1\%$) and D-Ser, D-Gln, and Gly (0.1-0.2% vs D-Asp, Supplementary Table 2). hDASPO shows a 5- and > 10 -fold higher specific activity than the homologous bovine enzyme and the orthologous flavoenzyme human D-amino acid oxidase (hDAAO, active on D-Ser), respectively (31,42).

Gel-permeation chromatography shows that recombinant hDASPO elutes as a single peak corresponding to a molecular mass of $\sim 39.2 \text{ kDa}$ (the expected mass for the hDASPO holoenzyme: 38647 Da), i.e., as a monomeric protein in the 0.1-15 mg/mL concentration range (Table 1), in agreement with the result by (43). The oligomerization state of hDASPO differs from that of pig and yeast DASPOs (which are tetramers) (44) and from that of the homologous DAAOs and eukaryotic L-amino acid oxidases, which are stable homodimers in solution (31,45,46).

The purified hDASPO shows the canonical absorbance spectrum of FAD-containing flavoproteins (Fig. 1A). The oxidized form of hDASPO is fully converted into the reduced state by adding aerobically the reducing agent dithionite ($K_d = 419 \pm 33 \text{ \mu M}$) or by a > 2 -fold molar excess of D-Asp under anaerobic conditions (Fig. 1A). hDASPO is photoreduced in the presence of 5 mM EDTA and 60 nM 5-deazaflavin at pH 8.0, forming a high amount (78%) of red anionic semiquinone (Fig. 1B). The conversion of the semiquinone species into a complete reduced form at longer illumination time (Fig. 1B, dotted lines and inset) points to a kinetic stabilization of the anionic flavin semiquinone, as observed with other flavoenzymes (47). For details, see Supplementary Data 1.

Structure of hDASPO

The wild-type hDASPO and several cysteine variants were tested for crystallization. Only the C141Y and C143G variant produced crystals suitable for X-ray analysis (named hDASPO*, Fig. 2, see Methods and Supplementary Data 2 for the details about the selection of cysteine residues to generate hDASPO variants for protein crystallization). The maximal activity of hDASPO* on D-Asp (at 21% oxygen saturation) is ~ 15% slower than for the wild-type enzyme, while the thermal stability of this variant resembles that of the wild-type protein (Supplementary Table 3); therefore only minor structural changes are expected as a result of the amino acid substitutions. Crystals of hDASPO* diffracted to 3.22 Å resolution (Supplementary Table 1) and the 3D structure was solved by molecular replacement using the hDAAO structure as the search model.

The hDASPO* structure is divided into two domains, the FAD-binding domain (FBD: residues 1-46, 143-192, 282-335) with the canonical dinucleotide binding fold observed in several flavoenzymes (48), and the substrate-binding domain (SDB: residues 47-142, 193-281) characterized by a large, eight-stranded, mixed β -sheet (Fig. 3A).

A structural analysis using DALI (49) indicates that the hDASPO* tertiary structure resembles that of FAD-binding oxidoreductases, in particular DAAOs. The best match is obtained with hDAAO (PDB code 5ZJA; DALI Z-score of 45.2, residue identity of 41%), with an overall root mean square deviation of 1.4 Å. Worthy of note is the presence of insertions/deletions and poor residue conservation at three loops in the SBD (54-63, 101-107, 217-221) between hDASPO* and hDAAO (Fig. 2 and Fig. 3B). These differences have a major impact on the main-chain structure of the regions surrounding the substrate-binding site (see below). Despite the overall structural conservation between hDASPO* and hDAAO, the latter is dimeric in solution while hDASPO* is monomeric. Analysis of the protein surface of hDASPO* corresponding to the dimerization surface in the SBD of hDAAO reveals that single substitutions decrease the hydrophobicity (His90, Lys126, Ala135 in hDASPO *vs* Phe90, Met124, Phe133 in hDAAO) or change the polarity (Asn73, Asn80, Ala122 and Glu212 in hDASPO *vs* Asp73, His80, Arg120 and Lys211 in hDAAO) of this region (Fig. 2, Fig. 3C,D and Supplementary Fig. 2), thus favoring the hDASPO monomeric form in solution. Interestingly, a hDAAO-like dimeric arrangement is apparent in the hDASPO* crystal packing, where the quaternary assembly formation is mediated by the presence of a phosphate ion and a Tris molecule (derived from the protein buffer) that fit into two small cavities at the dimeric interface (Fig. 3C). Such a region in hDAAO is filled by residues directly involved in protein-protein packing (Phe133 and Lys211 in hDAAO *vs* Ala135 and Glu212 in hDASPO, Fig. 2 and Supplementary Fig. 2).

In conclusion, hDASPO* belongs to the FAD-binding oxidoreductase structure family, similar to hDAAO, but with insertions/deletions and site-specific substitutions that alter the oligomerization state and substrate-binding site of hDASPO* in comparison to hDAAO (see below).

Cofactor binding

FAD binds to hDASPO* in an extended conformation (Fig. 3A,B and Supplementary Fig. 3), matching that found in DAAOs (50-54) and structurally related FAD-binding proteins (55). The flavin ring is located at the interface between FBD and SBD, with nearly all hydrogen-bond donors and acceptors of FAD interacting with protein atoms. Thirty-five residues are directly involved in FAD binding (at a distance below 4.5 Å), eight of which establish electrostatic or polar interactions with the cofactor. Only three of the latter interactions involve side-chain atoms (residues Ser44, Thr43, and Ser312), the others being due to atoms belonging to the backbone (Fig. 2 and Supplementary Fig. 3). The N-terminal dipoles of helices A11 and A1 point toward the O2 position of the isoalloxazine ring and the pyrophosphate group of FAD, respectively. These two dipoles represent a typical structural fingerprint of glutathione reductase 2 family (55).

The flavin ring does not show any significant deviation from planarity and it is held in place by several interactions with the protein (Supplementary Fig. 3). The most conserved FAD-protein interactions in the six hDASPO* molecules of the crystal asymmetric unit are between the N1 atom and Ser308, O2 atom and Ser312, and N3 atom and Met50, while the interactions O4-Met50 and N5-Ala48 are less conserved. The benzene ring of the flavin extensively interacts with the protein and its two methyl groups are in van der Waals contact with Val203 and Gly276. Overall, the FAD-binding mode of hDASPO* resembles that found in hDAAO, with a remarkable difference at the FAD ribose moiety, mostly due to the presence of hDASPO Gly186 instead of the corresponding Trp185 in hDAAO (Fig. 3).

Flavin binding modulates the conformation and stability of hDASPO. Gel-permeation chromatography indicates that the apoprotein form of hDASPO is present in solution as a 2:1 molar ratio between a monomeric (~ 39 kDa) and a trimeric species (100 ± 7 kDa). Circular dichroism (CD) measurements indicate that both the secondary structure (a 5% lower α -helix content was predicted from the near-UV CD spectra, Supplementary Fig. 4A) and tertiary structure of the hDASPO apoprotein (see the far-UV CD spectra in Supplementary Fig. 4B) are altered compared with the holoenzyme. Thermal stability of hDASPO is increased by the presence of the cofactor (the apoprotein form is slightly less stable than the holoenzyme, which is further stabilized by an excess of free FAD) or by a saturating 5-An concentration (Table 1, Supplementary Fig. 5). Interestingly, a synergistic effect is apparent: in the presence of 1 mM 5-An and 60 μ M FAD a 15.3 °C increase in T_m is observed. These results indicate a slightly lower thermal stability of hDASPO compared with hDAAO and a similar stabilization by the presence of a ligand at the active site of the enzyme (56).

The FAD dissociation constant (K_d) was determined from changes in hDASPO fluorescence intensity during titration of the apoprotein with FAD (Supplementary Fig. 6): a K_d of 33 ± 2.7 nM was estimated. The presence of tartrate (a known active-site ligand of bovine DASPO) (57) marginally affects the affinity of hDASPO for

the cofactor (K_d of 68 ± 1 nM). Notably, this result is the opposite of that of the ~ 25 -fold tighter FAD binding observed for hDAAO in the presence of the active-site ligand benzoate (31), a difference mainly due to the different active-site loops (see below). Based on the estimated K_d value and brain FAD concentration (~ 2.5 μ M) (58), hDASPO should exist *in vivo* largely in the active, holoenzyme form, while for the orthologue hDAAO the inactive apoprotein represents the predominant form. The kinetics of holoenzyme reconstitution is reported in Supplementary Data 3.

Binding of ligands (and substrate specificity)

In hDASPO* the substrate-binding site can be described as a cavity lined by hydrophobic (Ala48, Met50, Ile52, Tyr223, and Tyr225) and charged (His54, Arg216, Arg237, Arg278, and Ser308) side chains, the latter residues being clustered at the entrance of the active site (Fig. 4D). Despite the fact that the overall shape and geometry of the active site show some similarities to hDAAO, several remarkable differences are evident. In hDASPO*, Tyr223 and Arg278 perfectly superimpose to hDAAO Tyr228 and Arg283, which are responsible for binding the substrate α -carboxylate group juxtaposed to the flavin C6 atom (54), suggesting a similar D-aspartate α -carboxylate binding mode for hDASPO*. Indeed, electron density shows the presence of a small ligand in the hDASPO* active site which was modeled as a glycerol molecule, possibly derived from the cryoprotectant solution (Fig. 4B, and Supplementary Fig. 3B). In contrast, the loop 217-221 in hDASPO*, which shapes the active-site surface at the interface with the solvent region, is much shorter than in hDAAO (residues 216-226), due to a six-residue deletion (Fig. 2 and Fig. 3B). In hDAAO this loop forms a lid covering and gating the substrate-binding site, and providing Tyr224, whose side chain builds the roof of the substrate-binding site (50,59). The conformational movement of this lid loop limits the turnover number of mammalian DAAOs as compared to the yeast counterpart, where it is absent (14.7 and 350 s^{-1} , respectively) (52,59). In hDASPO* this loop region is totally reshaped, with the hDAAO Tyr224 side chain being replaced by His54 and Arg237 side chains. These residues, together with Arg216, create a positive surface cleft at the entrance of the active site, able to attract the negatively charged D-Asp substrate (Fig. 4D).

Worthy of note, the His54 and Arg237 side chains show two distinct conformations in the six hDASPO* molecules of the crystal asymmetric unit, pointing toward the internal (close conformation) or the external (open conformation) part of the substrate-binding cavity (Fig. 4E). A certain degree of structural variability is also apparent for the Arg237 side chain, while Arg216 is more rigid, thus suggesting a putative active-site gating role for His54 and Arg237. Interestingly, while enzymatic activity of hDASPO is identical in the absence and in the presence of 10% glycerol, it decreases ($\sim 50\%$) in the presence of 20% glycerol. The inverse correlation between the buffer viscosity and enzymatic activity is in agreement with the proposed

conformational change of residues His54 and Arg237 required for substrate/product exchange at the active site of the enzyme.

Furthermore, docking of the D-Asp substrate indicates that His54, Arg237, and Arg278 side chains shape the active-site internal pocket responsible for stabilizing the negatively charged D-Asp side chain (Fig. 4C). A D-Glu substrate would, instead, clash against the side chains of Arg216 and Tyr225, in agreement with the hDASPO specificity for D-Asp. Furthermore, the pocket lined by Ile52, His54, and Ser308 is wide enough to accommodate the methyl group of the NMDA substrate. The negatively charged α -carboxylic group of the substrate interacts with the positively charged Arg278 and with the hydroxyl oxygen of Tyr223, and the α -H of the substrate pointing toward N(5) of FAD, an ideal setup for promoting an efficient hydride transfer during cofactor reduction (Fig. 4C). The substrate-binding network is completed by the H-bond interaction of the α -amino group of the substrate with the carbonyl oxygen of Ser308 and/or the His54 side chain.

The binding to hDASPO of various compounds known as D- and L-amino acid oxidase active-site ligands (60) was investigated by a spectrophotometric approach (56). The plot of the absorbance change at 501 nm as a function of the 5-An concentration showed a hyperbolic behavior with a $K_d = 10.2 \pm 2.4 \mu\text{M}$ (Fig. 5A and Table 1), a value slightly higher than the K_i value previously reported ($K_i = 3.80 \pm 0.96 \mu\text{M}$) (28). The docking analysis of 5-An shows that the ligand planar ring is parallel to the His54 side-chain ring while the carboxyl group of 5-An has a tilted orientation in comparison with the Arg278 guanidinium group due to the steric hindrance of the hydroxyl groups of Tyr223 and Ser308 side chains (Fig. 5A). hDASPO binds two of the three stereoisomers of the classical DASPO inhibitor tartrate (42), with a K_d of 0.87 mM and 0.06 mM for L-(+)-tartrate and meso-tartrate (MT), respectively (Fig. 5B and Supplementary Fig. 7). These latter value is 2-fold higher than the binding of MT to the bovine enzyme ($K_d = 26.5 \mu\text{M}$) (42), which has a proline instead of the His54 present in hDASPO (Fig. 2). Interestingly, hDASPO also binds two hDAAO inhibitors, 6-chloro-1,2-benzoxazol-3-one (CBIO) and pyrido[2,3-b]pyrazine-2,3(1H,4H)-dione (DPPD), which decreases the 453 nm absorbance peak and causes a bathochromic shift up to 468 nm (Fig. 5C and Supplementary Fig. 7). The K_d are 50.8 and 23.4 μM , respectively (Table 1), indicating that these molecules are better suited to bind hDAAO ($K_d = 0.19 \mu\text{M}$ and 1 μM for the CBIO- and DPPD-hDAAO complexes) (61). Docking analysis shows that the DPPD rings do not lie parallel to the isoalloxazine ring system of FAD because of the steric hindrance of Ser308 carbonyl oxygen and of the side chain of Ile52 (Fig. 5C). hDASPO also binds the canonical hDAAO inhibitors such as benzoate and anthranilate (two aromatic carboxylic acids) (Table 1 and Supplementary Fig. 7). None of these D- and L-amino acid oxidases active-site ligands appears strong enough to produce a hDASPO inhibition effect *in vivo* (see below).

Site-directed mutagenesis of His54 and Arg237

In order to support the proposed gating role of residues His54 and Arg237, which show alternative orientations in the different monomers of the asymmetric unit, the H54A and R237A hDASPO variants were generated. Both enzyme variants showed a lower maximal activity and kinetic efficiency compared to the wild-type hDASPO for all tested D-amino acids except for H54A on D-Asn (~ 50% higher apparent kinetic efficiency) and NMDA (see below). In particular, a significant increase in $K_{m,app}$ was apparent for the R237A variant on D-Asp (up to ~ 20-fold, Supplementary Table 4). These findings suggest that these residues, that must adopt an 'open' conformation to allow the binding of the substrate and the release of the product, switch to a 'closed' conformation to interact with the substrate/ligand when it occupies the active site. For all hDASPO variants very similar kinetic parameters were determined for D-Glu, indicating that the lower affinity for this substrate is probably due to clashes with Arg216 and Tyr225 (see above). Notably, the H54A hDASPO showed the highest apparent maximal activity and affinity for NMDA pointing to an enlargement of the active site region that accommodate the N-methyl group of NMDA (Supplementary Table 4).

Concerning ligand binding, the K_d values for the three representative active site ligands 5-An, CBIO and MT were increased for both H54A and R237A hDASPO variants compared to the wild-type counterpart (Table 1). The largest increase was apparent for the latter variant and MT due to the loss of the electrostatic interaction between a carboxylate of the ligand and the side chain of the residue at position 237 (K_d of 191 μ M for R237A vs. 57 μ M for wild-type hDASPO).

Kinetic mechanism

The kinetic mechanism of hDASPO was investigated using D-Asp as substrate by both the enzyme-monitored turnover method (EMTN) as a function of oxygen concentration and by the rapid kinetic approach using a stopped-flow spectrophotometer (detailed in Supplementary Data 4) (62).

In EMTN, the oxidized enzyme was mixed aerobically with increasing amounts of D-Asp and the changes in flavin absorption monitored at 450 nm (see Supplementary Fig. 8). The double reciprocal plot of observed rate vs. O_2 concentration (inset of Supplementary Fig. 8) shows a set of lines converging on the negative abscissa: this behavior is compatible with formation of a ternary complex mechanism (63). Compared to bovine DASPO, the $K_{m,D-Asp}$ and k_{cat} values are ~5-fold higher (Table 2), suggesting a different rate-limiting step in catalysis.

The reductive half-reaction (studied by anaerobically mixing hDASPO with increasing concentrations of D-Asp and recording the absorption spectra during the reaction, Fig. 6A,B) shows a full flavin reduction only at D-Asp concentrations ≥ 2.5 mM, suggesting that the reductive half-reaction is reversible. This was confirmed by static anaerobic titration of reduced enzyme with oxaloacetate (OA) in the presence of 8.5 mM ammonium chloride to generate the product iminoaspartate (IASp): FAD was reoxidized by adding OA and reduced again by adding further D-Asp (Supplementary Fig. 9A). Assuming that all OA is converted into IASp at the fixed ammonium

chloride concentration used, an equilibrium constant of 4.7 ± 1.3 was estimated for the overall $E_{ox} + D\text{-Asp} \leftrightarrow E_{red} + I\text{Asp}$ process. The absorbance change at 450 nm during anaerobic reduction at increasing D-Asp concentrations is biphasic: the second, slow phase is insensitive to D-Asp concentration and disappears at high D-Asp concentration. The step of IAsp release from the reduced $E\text{-FAD}_{red}\text{-IAsp}$ complex is not evident in stopped-flow experiments (k_3 in the scheme in Fig. 6 top). A direct plot of the observed rates for the first phase of reduction, k_{obs1} , at increasing D-Asp concentration shows a hyperbolic behavior (Fig. 6B), which describes a first-order reaction of a binary complex (k_2/k_{-2}) that follows a second-order complex formation (k_1/k_{-1}) (64). A k_{red} (k_2) of 1550 s^{-1} was estimated (at $25 \text{ }^\circ\text{C}$), a value 10-fold higher than the k_{cat} value, indicating that the substrate oxidation step is not rate limiting in catalysis (Table 2). The inferred value resembles (considering the different temperature) that calculated for bovine DASPO ($k_{red} = 180 \text{ s}^{-1}$ at $4 \text{ }^\circ\text{C}$) (55). Indeed, the apparent K_d for D-Asp (23 mM), which is also similar to the value for bovine DASPO and hDAAO (for D-Ala; see Table 2), suggests that the substrate concentration largely controls the reaction rate.

The oxidative half-reaction was investigated by mixing the substrate-reduced hDASPO with a buffer saturated at increasing oxygen concentrations and recording the absorbance at $25 \text{ }^\circ\text{C}$ (Fig. 6C,D). An increase in the 453 nm absorbance is observed that was satisfactorily fitted with a single exponential process: a reoxidation rate constant of $\sim 10 \times 10^4 \text{ M}^{-1}\text{s}^{-1}$ was calculated (Table 2). The presence of 3.35 mM MT or of 1 mM OA, to mimic the presence of the substrate/product in the active site, does not significantly alter the reoxidation rate (Supplementary Fig. 10).

The kinetic mechanism of hDASPO follows a ternary complex mechanism characterized by a very fast step of flavin reduction followed by a rate-limiting reoxidation step. The mechanism of hDASPO differs from that of the bovine counterpart: the reoxidation rate of the reduced enzyme is significantly faster and no binding of a second molecule of D-Asp or of a related, rate-limiting, conformational change is evident (57).

DISCUSSION

The investigation of D-amino acids sheds light on several relevant physiological functions involving these atypical molecules (4,6) and on their contribution to human pathological states. Here, the agonistic effect of D-Asp at NMDAR and its ability to improve cognition and protect against sensorimotor gating deficits due to psychotomimetic drugs in preclinical models highlight its relevance in physiological conditions and neuropsychiatric disorders (15,21,65,66). In this work we investigated the structure-function relationships of hDASPO, the only human enzyme known to degrade D-Asp, in order to elucidate D-Asp metabolism.

hDASPO belongs to the family of amino acid oxidase flavoproteins and sequence analysis reveals homology with hDAAO (Fig. 2), which is involved in degradation of D-Ser in the brain, the main coagonist of NMDAR (7). hDASPO and hDAAO profoundly differ in quaternary structure, substrate-binding site entrance, FAD

affinity, kinetic properties (i.e., maximal activity) and mechanism, although they share a similar overall tertiary structure (Fig. 3 and Supplementary Fig. 2). These striking differences result in two different modes of modulation of the brain levels of D-Asp and D-Ser by the two orthologue flavoenzymes.

hDASPO is a monomeric, 39-kDa holoenzyme, while hDAAO is an 80-kDa homodimer. Interestingly, we identified a vestigial dimeric surface in hDASPO* crystals, stabilized by exogenous molecules (Tris and phosphate ion), similar to hDAAO (Fig. 3C,D). However, specific sequence variations at the protein-protein interface, in terms of both hydrophobic and polar residue distribution, justify the monomeric state of hDASPO in solution (Fig. 2 and Supplementary Fig. 2). This mode of molecular evolution of the dimerization interface was also observed comparing human and rat DAAO (67). The different quaternary structure can affect both subcellular trafficking (passive translocation into mammalian cell nuclei has a diffusion limit of 40 kDa) and modulation by interacting proteins - such as by pLG72, the main hDAAO interacting partner (68,69), which also binds hDASPO (unpublished result).

From the analysis of the 3D structure, we can conclude that binding of the α -carboxylate of the substrate occurs in hDASPO through the interaction with Tyr223 and Arg278, similar to hDAAO, whereas the D-Asp side chain fits a positively charged pocket lined by His54, Arg216, and Arg237. This highly conserved region, which is specific to DASPO enzymes (Fig. 2), is located close to the entrance of the active site and fulfils two main functions: (i) it creates an electrostatic funnel facilitating D-Asp entrance and (ii) stabilizes the substrate side chain into the active site (Fig. 4). This double function is supported by the decreased interaction observed for D-Asp or ligand binding to H54A and R237A hDASPO variants and by the multiple conformations of the Arg and His residues observed in the different hDASPO molecules of the crystal asymmetric unit, with side chains facing the interior or the exterior of the active site in different protomers. This active-site gating role of the Arg-His system (which allows substrate entry and interaction during catalysis) is coupled with a drastic shortening in hDASPO of the loop region, which in hDAAO acts as an active-site lid (Fig. 2 and Fig. 3B). This structural difference i) narrows the substrate scope as hDASPO is mainly active on D-Asp while it shows a very low activity toward D-Glu (and a low affinity for known hDAAO inhibitors, see Table 1) and ii) facilitates substrate/product exchange, thus improving the hDASPO activity. The role of Arg216 in substrate selectivity is apparent by the lower kinetic efficiency reported for the R216Q hDASPO variant on D-Asp and the gained ability to oxidized D-Ala (29). The residue at position 54 seems to be also involved in ligand selectivity: a lower $K_{m,app}$ for NMDA ensues from introducing an alanine (compare H54A vs. wild-type hDASPO) and the presence of a proline results in a 2-fold lower K_d for binding of MT (such as in the bovine DASPO) (42).

As a matter of fact, the conformational change of the active-site lid during catalysis limits the turnover number of mammalian DAAOs, see Table 2 (50). The rate-limiting step for bovine DASPO corresponds to a conformational change related to the binding of a second molecule of D-Asp to the reduced enzyme form (57),

while for hDAAO it has been identified as the flavin reduction step (31). In contrast, the rate-limiting step of the enzymatic reaction in hDASPO is reoxidation of the reduced flavin. Notably, the activity of hDASPO is significantly higher than that of hDAAO (as well as of bovine DASPO). Both oxidases involved in the degradation of the brain D-amino acid neuromodulators show a low affinity for their substrates (D-Asp and D-Ser, respectively): K_m and K_d values are in the millimolar range, indicating that at physiological concentrations (lower than 1 mM) the enzymatic activity directly depends on the substrate concentration.

hDAAO shows a weak FAD interaction (K_d in the micromolar range, see Table 1) and thus exists in solution as an equilibrium between the active holoenzyme and the inactive apoprotein. Furthermore, binding of an active-site ligand (as well as the substrate) facilitates FAD binding, yielding a higher amount of hDAAO holoenzyme and thus pushing D-Ser degradation (3259). Such a modulation of the catabolic activity by ligand binding is not present in hDASPO since the strong interaction with the FAD cofactor ($K_d = 3\text{-}7 \times 10^{-8}$ M, a value 30-fold lower than the bovine counterpart) (42) yields a stable holoenzyme. From the structural viewpoint, the protein-FAD interactions are very similar in the two oxidases, with only minor variations at the adenosine moiety; therefore, a different affinity for the cofactor could be ascribed to different dynamics of flavin binding more than to specific interactions. Actually, the binding of a ligand in hDAAO results in a conformational change of the flexible lid at the entrance of the active site which, in turn, could stabilize the holoenzyme conformation. This mechanism was not observed in hDASPO and in yeast DAAO (51,52), which both lack such a lid region.

Overall, structural and functional data highlight that hDASPO significantly differs from hDAAO, pointing to a diverging evolution driven by different metabolic requirements. hDASPO is a specific and efficient catabolic enzyme that strictly controls D-Asp cellular concentration. In mammalian brain, the occurrence of D-Asp is transient: it is highly concentrated during the embryonic stage (reaching $0.36 \mu\text{mol/g}$ at gestational week 14) and it strongly decreases after the first days of life when DASPO is expressed (70). DASPO knockout mice show 10- to 20- fold higher D-Asp levels in the brain (15,22). Indeed, oral administration of D-Asp requires a chronic treatment with 20 mM D-amino acid solution for one month to reach a significant increase in the level of this neurotransmitter (22,24). While control of D-Asp levels in the brain requires an efficient “scavenger” enzyme, D-Ser levels are modulated by an evolution-related flavoenzyme characterized by a low activity and which is unable to deplete the NMDAR coagonist.

Our studies make it now conceivable that cellular D-Asp levels acting on the catabolism of this neuromodulator can be increased. In particular, the 3D structure of hDASPO allows to devise a pipeline for rational design of selective inhibitors consisting of: (i) *in silico* screening of clinically exposed compounds/drugs (drug repurposing) and small molecules that could bind to hDASPO and interfere with its enzymatic activity; (ii) chemical improvement of known hDAAO ligands for hDASPO inhibition; (iii) experimental confirmation/validation of enzymatic inhibition by *in vitro* and cell experiments. The selected hit compounds, in

the medium long term, could be chemically engineered to become potential innovative antipsychotic drugs to treat neurological diseases related to NMDAR dysfunction, such as schizophrenia, as well as to stimulate myelin repair in the disability associated with multiple sclerosis

ACKNOWLEDGEMENTS

We acknowledge access to the i04 beamline at the Diamond light source. We thank dr. Silvia Sacchi and dr. Valentina Rabattoni for helpful discussions.

AUTHOR CONTRIBUTIONS

LP and GM initiated the study and directed the biochemical part of the work. AS performed the purification and biochemical characterization of wild-type and variants hDASPO under the supervision of GM and of LP (for the kinetic studies). AC and MN conducted the crystallographic and computational analyses. AS and AC prepared the figures. LP, GM, and MN prepared the manuscript, which was revised and approved by all authors.

Additional information

Supplementary Data 1 to 4

Supplementary Figs. 1 to 10

Supplementary Tables 1 to 4

REFERENCES

1. Errico, F., Napolitano, F., Nisticò, R., Centonze, D., and Usiello A. (2009) D-aspartate: an atypical amino acid with neuromodulatory activity in mammals. *Rev. Neurosci.* **20** 429-440
2. Sasabe, J., and Suzuki, M. (2018) Emerging role of D-amino acid metabolism in the innate defense. *Front. Microbiol.* **9** 933
3. Aliashkevich, A., Alvarez, L., and Cava, F. (2018) New insights into the mechanisms and biological roles of D-amino acids in complex eco-systems. *Front. Microbiol.* **9** 683
4. Katane, M., and Homma, H. (2010) D-aspartate oxidase: the sole catabolic enzyme acting on free D-aspartate in mammals. *Chem. Biodivers.* **7** 1435-1449.
5. Ota, N., Shi, T., and Sweedler J.V. (2012) D-aspartate acts as a signaling molecule in nervous and neuroendocrine systems. *Amino Acids* **43** 1873-1886
6. Guercio, G.D., and Panizzutti, R. (2018) Potential and challenges for the clinical use of D-serine as a cognitive enhancer. *Front. Psychiatry* **9** 14
7. Pollegioni, L., and Sacchi, S (2010) Metabolism of the neuromodulator D-serine. *Cell. Mol. Life Sci.* **67**

8. Wolosker, H. (2011) Serine racemase and the serine shuttle between neurons and astrocytes. *Biochim. Biophys. Acta* **1814** 1558-1566
9. Wolosker, H., D'Aniello, A., and Snyder, S.H. (2000) D-aspartate disposition in neuronal and endocrine tissues: ontogeny, biosynthesis and release. *Neuroscience* **100** 183-189
10. Ota, N., Shi, T., Sweedler, J.V. (2012) D-Aspartate acts as a signaling molecule in nervous and neuroendocrine systems. *Amino Acids* **43** 1873-1886
11. Di Fiore, M.M., Santillo, A., Chieffi Baccari, G. (2014) Current knowledge of D-aspartate in glandular tissues. *Amino Acids* **46** 1805-1818
12. Schell, M.J., Cooper, O.B., and Snyder, S.H. (1997) D-aspartate localizations imply neuronal and neuroendocrine roles. *Proc. Natl. Acad. Sci. USA* **94** 2013-2018
13. Errico, F., Napolitano, F., Nisticò, R., and Usiello, A. (2012) New insights on the role of free D-aspartate in the mammalian brain. *Amino Acids* **43** 1861-1871
14. Hashimoto, A., Kumashiro, S., Nishikawa, T., Oka, T., Takahashi, K., Mito, T., Takashima, S., Doi, N., Mizutani, Y., Yamazaki, T., Kaneko, T., and Ootomo, E. (1993) Embryonic development and postnatal changes in free D-aspartate and D-serine in the human prefrontal cortex. *J. Neurochem.* **61** 348-351
15. Errico, F., Nisticò, R., Napolitano, F., Mazzola, C., Astone, D., Pisapia, T., Giustizieri, M., D'Aniello, A., Mercuri, N.B., and Usiello, A. (2011) Increased D-aspartate brain content rescues hippocampal age-related synaptic plasticity deterioration of mice. *Neurobiol. Aging* **32** 2229-2243
16. Ito, T., Hayashida, M., Kobayashi, S., Muto, N., Hayashi, A., Yoshimura, T., and Mori, H. (2016) Serine racemase is involved in D-aspartate biosynthesis. *J. Biochem.* **160** 345-353
17. Zaar, K., Köst, H.P., Schad, A., Völkl, A., Baumgart, E., and Fahimi, H.D. (2002) Cellular and subcellular distribution of D-aspartate oxidase in human and rat brain. *J. Comp. Neurol.* **450** 272-282
18. D'Aniello, S., Somorjai, I., Garcia-Fernández, J., Topo, E., and D'Aniello, A. (2011) D-aspartic acid is a novel endogenous neurotransmitter. *FASEB J.* **25** 1014-1027
19. Molinaro, G., Pietracupa, S., Di Menna, L., Pescatori, L., Usiello, A., Battaglia, G., Nicoletti, F., and Bruno, V. (2010) D-aspartate activates mGlu receptors coupled to polyphosphoinositide hydrolysis in neonate rat brain slices. *Neurosci. Lett.* **478** 128-130
20. Cristino, L., Luongo, L., Squillace, M., Paolone, G., Mango, D., Piccinin, S., Zianni, E., Imperatore, R., Iannotta, M., Longo, M., Errico, F., Vescovi, A.L., Morari, M., Maione, S., Gardoni, F., Nisticò, R., and Usiello, A. (2015) D-aspartate oxidase influences glutamatergic system homeostasis in mammalian brain. *Neurobiol. Aging* **36** 1890-1902
21. Errico, F., Napolitano, F., Squillace, M., Vitucci, D., Blasi, G., de Bartolomeis, A., Bertolino, A., D'Aniello,

- A., and Usiello, A. (2013) Decreased levels of D-aspartate and NMDA in the prefrontal cortex and striatum of patients with schizophrenia. *J. Psychiatr. Res.* **47** 1432-1437
22. Errico, F., Nisticò, R., Palma, G., Federici, M., Affuso, A., Brillì, E., Topo, E., Centonze, D., Bernardi, G., Bozzi, Y., D'Aniello, A., Di Lauro, R., Mercuri, N.B., and Usiello, A. (2008) Increased levels of D-aspartate in the hippocampus enhance LTP but do not facilitate cognitive flexibility. *Mol. Cell. Neurosci.* **37** 236-246
23. D'Aniello, A., Luongo, L., Romano, R., Iannotta, M., Marabese, I., Boccella, S., Belardo, C., de Novellis, V., Arra, C., Barbieri, A., D'Aniello, B., Scandurra, A., Magliozzi, L., Fisher, G., Guida, F., and Maione, S. (2017) D-aspartic acid ameliorates painful and neuropsychiatric changes and reduces β -amyloid A β . *Neurosci. Lett.* **651** 151-158
24. De Rosa, V., Secondo, A., Pannaccione, A., Ciccone, R., Formisano, L., Guida, N., Crispino, R., Fico, A., Polishchuk, R., D'Aniello, A., Annunziato, L., and Boscia, F. (2019) D-aspartate treatment attenuates myelin damage and stimulates myelin repair. *EMBO Mol. Med.* **11**(1) pii: e9278
25. Setoyama, C., and Miura, R. (1997) Structural and functional characterization of the human brain D-aspartate oxidase. *J. Biochem.* **121** 798-803
26. Katane, M., Kawata, T., Nakayama, K., Saitoh, Y., Kaneko, Y., Matsuda, S., Saitoh, Y., Miyamoto, T., Sekine, M., and Homma, H. (2015) Characterization of the enzymatic and structural properties of human D-aspartate oxidase and comparison with those of the rat and mouse enzymes. *Biol. Pharm. Bull.* **38** 298-305
27. Katane, M., Kuwabara, H., Nakayama, K., Saitoh, Y., Miyamoto, T., Sekine, M., and Homma, H. (2018) Rat D-aspartate oxidase is more similar to the human enzyme than the mouse enzyme. *Biochim. Biophys. Acta Proteins Proteom.* **1866** 806-812
28. Katane, M., Yamada, S., Kawaguchi, G., Chinen, M., Matsumura, M., Nakayama, K., Matsuda, S., Saitoh, Y., Miyamoto, T., Sekine, M., Yamaotsu, N., Hirono, S., and Homma, H. (2015) Identification of novel D-aspartate oxidase inhibitors by in silico screening and their functional and structural characterization in vitro. *J. Med. Chem.* **58** 7328-7340
29. Katane, M., Kanazawa, R., Kobayashi, R., Oishi, M., Nakayama, K., Saitoh, Y., Miyamoto, T., Sekine, M., and Homma, H. (2017) Structure-function relationships in human D-aspartate oxidase: characterisation of variants corresponding to known single nucleotide polymorphisms. *Biochim. Biophys. Acta Proteins Proteom.* **1865** 1129-1140
30. Hefti, M.H., Vervoort, J., and van Berkel, W.J. (2003) Deflavination and reconstitution of flavoproteins. *Eur. J. Biochem.* 2003 **270** 4227-4242
31. Molla, G., Sacchi, S., Bernasconi, M., Pilone, M.S., Fukui, K., and Pollegioni, L. (2006) Characterization of human D-amino acid oxidase. *FEBS Lett.* **580** 2358-2364
32. Caldinelli, L., Molla, G., Sacchi, S., Pilone, M.S., and Pollegioni, L. (2009) Relevance of weak flavin

- binding in human D-amino acid oxidase. *Protein Sci.* **18** 801-810
33. Gibson, Q.H., Swoboda, B.E., and Massey, V. (1964) Kinetics and mechanism of action of glucose oxidase. *J. Biol. Chem.* **239** 3927-3934
34. Senda, M., Yamamoto, A., Tanaka, H., Ishida, T., Horiike, K., and Senda, T. (2012) Crystallization and preliminary crystallographic analysis of D-aspartate oxidase from porcine kidney. *Acta Crystallogr. Sect. F Struct. Biol. Cryst. Commun.* **68** 644-646
35. Kabsch, W. (2010) XDS. *Acta Crystallogr. D Biol. Crystallogr.* **66** 125-132
36. Tickle, I.J. (2010) STARANISO, Cambridge, United Kingdom: Global Phasing Ltd. (2018)
37. Emsley, P., and Cowtan, K. (2004) Coot: model-building tools for molecular graphics. *Acta Crystallogr. D Biol. Crystallogr.* **60** 2126-2132
38. Adams, P.D., Afonine, P.V., Bunkóczi, G., Chen, V.B., Davis, I.W., Echols, N., Headd, J.J., Hung, L-W., Kapral, G.J., Grosse-Kunstleve, R.W., McCoy, A.J., Moriarty, N.W., Oeffner, R., Read, R.J., Richardson, D.C., Richardson, J.S., Terwilliger, T.C., and Zwart, P.H. (2010) PHENIX: a comprehensive Python-based system for macromolecular structure solution. *Acta Crystallogr. D Biol. Crystallogr.* **66** 213-221
39. Chen, V.B., Arendall, W.B., Headd, J.J., Keedy, D.A., Immormino, R.M., Kapral, G.J., Murray, L.W., Richardson, J.S., and Richardson, D.C. (2010) MolProbity: all-atom structure validation for macromolecular crystallography. *Acta Crystallogr. D Biol. Crystallogr.* **66** 12-21
40. Trott, O., and Olson, A.J. (2010) AutoDock Vina: improving the speed and accuracy of docking with a new scoring function, efficient optimization, and multithreading. *J. Comput. Chem.* **31** 455-461
41. Hanwell, M.D., Curtis, D.E., Lonie, D.C., Vandermeersch, T., Zurek, E., and Hutchison, G.R. (2012) Avogadro: an advanced semantic chemical editor, visualization, and analysis platform. *J. Cheminform.* **4** 17.
42. Negri, A., Massey, V., and Williams, C.H. (1987) D-aspartate oxidase from beef kidney. Purification and properties. *J. Biol. Chem.* **262** 10026-10034
43. Katane, M., Hanai, T., Furuchi, T., Sekine, M., and Homma, H. (2008) Hyperactive mutants of mouse D-aspartate oxidase: mutagenesis of the active site residue serine 308. *Amino Acids* **35** 75-82
44. Takahashi, S., Takahashi, T., Kera, Y., Matsunaga, R., Shibuya, H., and Yamada, R.H. (2004) Cloning and expression in *Escherichia coli* of the D-aspartate oxidase gene from the yeast *Cryptococcus humicola* and characterization of the recombinant enzyme. *J. Biochem.* **135** 533-540
45. Pawelek, P.D., Cheah, J., Coulombe, R., Macheroux, P., Ghisla, S., and Vrieland, A. (2000) The structure of L-amino acid oxidase reveals the substrate trajectory into an enantiomerically conserved active site. *EMBO J.* **19** 4204-4215

46. Pollegioni, L., Molla, G., Campaner, S., Martegani, E., and Pilone, M.S. (1997) Cloning, sequencing and expression in *E. coli* of a D-amino acid oxidase cDNA from *Rhodotorula gracilis* active on cephalosporin C. *J. Biotechnol.* **58** 115-123
47. Massey, V., and Hemmerich, P. (1980) Active-site probes of flavoproteins. *Biochem. Soc. Trans.* **8** 246-257
48. Fraaije, M.W., and Mattevi, A. (2000) Flavoenzymes: diverse catalysts with recurrent features. *Trends Biochem. Sci.* **25** 126-132
49. Holm, L., and Rosenström, P. (2010) Dali server: conservation mapping in 3D. *Nucleic Acids Res.* **38** W545-549
50. Mattevi, A., Vanoni, M.A., Todone, F., Rizzi, M., Teplyakov, A., Coda, A., Bolognesi, M., and Curti, B. (1996) Crystal structure of D-amino acid oxidase: a case of active site mirror-image convergent evolution with flavocytochrome b2. *Proc. Natl. Acad. Sci. USA* **93** 7496-7501
51. Umhau, S., Pollegioni, L., Molla, G., Diederichs, K., Welte, W., Pilone, M.S., and Ghisla, S. (2000) The x-ray structure of D-amino acid oxidase at very high resolution identifies the chemical mechanism of flavin-dependent substrate dehydrogenation. *Proc. Natl. Acad. Sci. USA* **97** 12463-12468
52. Pollegioni, L., Diederichs, K., Molla, G., Umhau, S., Welte, W., Ghisla, S., and Pilone, M.S. (2002) Yeast D-amino acid oxidase: structural basis of its catalytic properties. *J. Mol. Biol.* **324** 535-546
53. Mörtl, M., Diederichs, K., Welte, W., Molla, G., Motteran, L., Andriolo, G., Pilone, M.S., and Pollegioni, L. (2004) Structure-function correlation in glycine oxidase from *Bacillus subtilis*. *J. Biol. Chem.* **279** 29718-29727
54. Kawazoe, T., Tsuge, H., Pilone, M.S., and Fukui, K. (2006) Crystal structure of human D-amino acid oxidase: context-dependent variability of the backbone conformation of the VAAGL hydrophobic stretch located at the si-face of the flavin ring. *Protein Sci.* **15** 2708-2717
55. Dym, O., and Eisenberg D. (2001) Sequence-structure analysis of FAD-containing proteins. *Protein Sci.* **10** 1712-1728
56. Caldinelli, L., Molla, G., Bracci, L., Lelli, B., Pileri, S., Cappelletti, P., Sacchi, S., and Pollegioni, L. (2010) Effect of ligand binding on human D-amino acid oxidase: implications for the development of new drugs for schizophrenia treatment. *Protein Sci.* **19** 1500-1512
57. Negri, A., Massey, V., Williams, C.H., and Schopfer, L.M. (1988) The kinetic mechanism of beef kidney D-aspartate oxidase. *J. Biol. Chem.* **263** 13557-13563
58. Decker, L.E., and Byerrum, R.U. (1954) The relationship between dietary riboflavin concentration and the tissue concentration of riboflavin-containing coenzymes and enzymes. *J. Nutr.* **53** 303-315
59. Pollegioni, L., Piubelli, L., Sacchi, S., Pilone, M.S., and Molla, G. (2007) Physiological functions of D-amino acid oxidases: from yeast to humans. *Cell. Mol. Life Sci.* **64** 1373-1394

60. Sacchi, S., Rosini, E., Pollegioni, L., Molla, G. (2013) D-amino acid oxidase inhibitors as a novel class of drugs for schizophrenia therapy. *Curr. Pharm. Des.* **19** 2499-2511
61. Ferraris, D., Duvall, B., Ko, Y.S., Thomas, A.G., Rojas, C., Majer, P., Hashimoto, K., and Tsukamoto, T. (2008) Synthesis and biological evaluation of D-amino acid oxidase inhibitors. *J. Med. Chem.* **51** 3357-3359
62. Pollegioni, L., Langkau, B., Tischer, W., Ghisla, S., and Pilone, M.S. (1993) Kinetic mechanism of D-amino acid oxidases from *Rhodotorula gracilis* and *Trigonopsis variabilis*. *J. Biol. Chem.* **268** 13850-13857
63. Dalziel, K. (1969) The interpretation of kinetic data for enzyme-catalysed reactions involving three substrates. *Biochem. J.* **114** 547-556
64. Strickland, S., Palmer, G., and Massey, V. (1975) Determination of dissociation constants and specific rate constants of enzyme-substrate (or protein-ligand) interactions from rapid reaction kinetic data. *J. Biol. Chem.* **250** 4048-4052
65. Weil, Z.M., Huang, A.S., Beigneux, A., Kimb, P.M., Molliver, M.E., Blackshaw, S., Young, S.G., Nelson, R.J., and Snyder, S.H. (2006) Behavioural alterations in male mice lacking the gene for D-aspartate oxidase. *Behav. Brain Res.* **171** 295-302
66. Palazzo, E., Luongo, L., Guida, F., Marabese, I., Romano, R., Iannotta, M., Rossi, F., D'Aniello, A., Stella, L., Marmo, F., Usiello, A., de Bartolomeis, A., Maione, S., and de Novellis, V. (2016) D-aspartate drinking solution alleviates pain and cognitive impairment in neuropathic mice. *Amino Acids* **48** 1553-1567
67. Frattini, L.F., Piubelli, L., Sacchi, S., Molla, G., and Pollegioni, L. (2011) Is rat an appropriate animal model to study the involvement of D-serine catabolism in schizophrenia? Insights from characterization of D-amino acid oxidase. *FEBS J.* **278** 4362-4373
68. Sacchi, S., Cappelletti, P., Giovannardi, S., and Pollegioni, L. (2011) Evidence for the interaction of D-amino acid oxidase with pLG72 in a glial cell line. *Mol. Cell. Neurosci.* **48** 20-28
69. Sacchi, S., Binelli, G., and Pollegioni, L. (2016) G72 primate-specific gene: a still enigmatic element in psychiatric disorders. *Cell. Mol. Life Sci.* **73** 2029-2039
70. Van Veldhoven, P.P., Brees, C., and Mannaerts, G.P. (1991) D-aspartate oxidase, a peroxisomal enzyme in liver of rat and man. *Biochim. Biophys. Acta* **1073** 203-208

Figure 1. Spectral properties of hDASPO. A) Visible absorbance spectra of hDASPO (~ 16 μ M) in the free oxidized (1), half- (2), reduced free form (3) and in the oxidized form complexed with 8.6 mM L-(+)-tartrate (dashed line), or 23 μ M 5-aminonicotinic acid (dotted line). The spectrum of semiquinone form (2) was recorded 5.5 min after anaerobic photoirradiation in the presence of 5 mM EDTA and 60 nM 5-deazaflavin. The spectrum of reduced hDASPO (3) was recorded 30 min after the anaerobic addition of 52.6 μ M D-Asp. Buffer: 20 mM Tris-HCl, pH 8.0, 10% glycerol at 15 °C. B) Photoreduction of hDASPO. 15.9 μ M of enzyme was made anaerobic and mixed with 5 mM EDTA and 60 nM 5-deazaflavin (1). Then the spectra were recorded after 1 (2), 2 (3), 4.5 (4) 5.5 (5), 8.5, 13.5 and 16.5 minutes of irradiation. The semiquinone disappearance at ~ 8.5 min of illumination is shown in dotted lines. Inset: plot of absorbance at 455 nm vs 377 nm for each spectrum.

Figure 2. Structure-based sequence alignment of DASPO family members and hDAAO. Sequence alignment of hDASPO (Q99489.1), yeast DASPO (Q75WF1), hDAAO (P14920), mouse DASPO (Q922Z0), bovine DASPO (P31228) and pig DASPO (A3KCL7). A secondary structure scheme of hDASPO is reported above. Structurally different SDB loops are in red for hDASPO and hDAAO. Residues at the dimerization interface and those interacting with FAD are shaded in green and yellow, respectively. Key divergent residues in hDASPO and hDAAO at the dimerization interface are indicated with green dots. Residues lining the hDASPO active site are shown with blue dots. The double residue substitution of hDASPO* is shaded in violet. The lacking sequence of hDASPO isoform 2 (*DDO-2*) is shown in bold.

Figure 3. Structure of hDASPO. A) Ribbon representation of the substrate binding domain (SDB) and the FAD binding domain (FBD), labeled and colored in gold and cyan, respectively. FAD molecule is represented as orange sticks and labeled. B) Superimposition of hDASPO and hDAAO in green and blue (FBD and SBD, respectively). Differences at SBD are highlighted as red loops in the hDASPO structure. C) hDASPO crystal packing, and D) hDAAO dimer. The dimeric counterparts are in gray. Tris and phosphate molecules are indicated with red arrows at the protein-protein interface of hDASPO.

Figure 4. hDASPO active site. A) Superposition of hDASPO and hDAAO active sites (color code as in Fig. 3). B) Glycerol molecule bound to hDASPO* in the active site. C) Docking of D-Asp in the active site of hDASPO*. The purple line indicates the distance (3.5 Å) between D-Asp α Ca and the N5 of FAD. Ligands and FAD are colored in pale blue and orange, respectively. Polar interactions were represented as dashed lines. D, E) hDASPO active site entrance. D) Electrostatic surface at the active site entrance (blue positively charged, and red negatively charged side chains). Glycerol and FAD are visible inside the protein through the active site entrance. E) Detailed view of side-chain flexibility at the active site entrance as derived by superimposing the

six hDASPO* molecules present in the crystal asymmetric unit. His54 and Arg237 different orientations are highlighted with red arrows. Different residues are in different colours. For clarity the glycerol molecule is not shown.

Figure 5. Ligand binding at the active site of hDASPO. A) 5-AN; B) meso-tartrate (MT); C) DPPD. Left panels: spectral changes during titration of hDASPO with the indicated ligand. Selected spectra obtained upon adding increasing concentrations of ligands are shown. Arrows indicate the direction of change at increasing ligand concentrations. Inset: fit of the data to a hyperbolic binding curve (solid line). Right panels: models of the hDASPO-ligand complex inferred by molecular docking. The receptor is chain A. Orange: FAD, pale blue: ligand. Predicted H-bonds are shown with dotted lines.

Figure 6. A,B) Reductive half-reaction of hDASPO. Top) Scheme of the reductive half-reaction of hDASPO (IAsp = iminoaspartate). A) Spectral courses of the anaerobic reduction of hDASPO (11 μ M) by adding 0.25 mM D-Asp at 10 °C, followed in a stopped-flow spectrophotometer. Spectra were recorded at 20 ms (1), 40 ms (2), 100 ms (3), 250 ms (4), 5 s (5) and 10 s (6) after mixing. Inset: time courses of anaerobic reduction of hDASPO followed at 450 nm after mixing with 0.125 mM (1), 0.25 mM (2), 0.5 mM (3), 1 mM (4), 2.5 mM (5), 5 mM (6) and 12.5 mM (7) D-Asp (final concentrations). Buffer: 100 mM disodium pyrophosphate pH 8.5, 1% glycerol, 2 mM D-Ala, 10 μ g/ μ L catalase. B) Dependence of the observed rate of anaerobic reduction of hDASPO on D-Asp concentration at 10 and 25 °C. Vertical bars indicate \pm SE for five determinations: when not shown, the standard error is smaller than the symbols used. C,D). Oxidative half-reaction of free reduced hDASPO, at 25 °C. Top) Scheme of the oxidative half-reaction of free, reduced hDASPO. C) Course of reoxidation of 12.2 μ M reduced hDASPO by 12.5% oxygen (final concentrations). The spectra were recorded 20 ms (1), 30 ms (2), 50 ms (3), 80 ms (4), 100 ms (5), 200 ms (6) and 500 ms (7) after mixing. D) Time course of the 453 nm absorbance intensity during the reaction of 12.2 μ M reduced hDASPO with 1.25% (1), 5% (2), 12.5% (3), 25% (4) and 50% (5) oxygen (final concentrations). Inset: linear fit of the observed rate constants (k_{obs}) obtained at each oxygen concentration. Buffer contained 2 mM D-Ala and 0.5 μ M RgDAAO.

Table 1

Biochemical and structural properties of hDASPO, compared with those for the homologous enzyme hDAAO (31,60,61).

	hDASPO	hDAAO
Oligomerization state:		
apoprotein	monomer-trimer equilibrium	dimer
holoenzyme	monomer	dimer
FAD binding, K_d (M):		
free form	$3.3 \pm 0.3 \times 10^{-8}$ [$1.1 \pm 0.1 \times 10^{-6}$] ^a	$8 \pm 2 \times 10^{-6}$
ligand complex	$6.8 \pm 0.3 \times 10^{-8}$ (L-(+)-tartrate)	$3 \pm 1 \times 10^{-7}$ (benzoate)
Ligand binding, K_d (mM):		
benzoate	7.8 ± 0.6 [69.5 ± 6.8] ^a	7×10^{-3}
anthranilate	8.8 ± 1.5 [9.0 ± 0.4] ^a	40×10^{-3}
CBIO	$5.1 \pm 0.5 \times 10^{-2}$ (10.9 ± 0.8 ; 11.6 ± 0.8) ^b	1.9×10^{-4}
meso-tartrate	$5.7 \pm 0.3 \times 10^{-2}$ (7.3 ± 0.5 ; 19.1 ± 1.0) ^b	n.d.
L-(+)-tartrate	$8.7 \pm 0.2 \times 10^{-1}$	n.d.
5-aminonicotinic acid	$10.1 \pm 2.4 \times 10^{-3}$ [$3.8 \pm 1.0 \times 10^{-3}$] ^a (12.7 ± 1.6 ; 15.1 ± 2.3) ^b	n.d.
DPPD	$31.5 \pm 7.5 \times 10^{-3}$	1×10^{-3} ^c
T_m (°C), far-UV CD (220 nm):		
apoprotein	45.6 ± 0.1	50.2 ± 1.5
free holoenzyme	48.8 ± 0.1	50.1 ± 1.2
holoenzyme + 60 μ M FAD	52.5 ± 0.2	51.8 ± 0.2
ligand complex: L-(+)-tartrate	54.2 ± 0.1	55.7 (benzoate)
Meso-tartrate	51.7 ± 0.1	n.d.
5-An (10x K_d)	53.3 ± 0.1	n.d.
5-An (100x K_d)	57.4 ± 0.2	n.d.
5-An (100x K_d) + 60 μ M FAD	64.1 ± 0.1	n.d.

n.d. = not determined

^a In square parentheses the K_i values for mDASPO (4,43)

^b In parentheses the K_d values for H54A and R237A hDASPO variants

^c IC_{50} value, unpublished result

Table 2

Steady state kinetic parameters and reduction and reoxidation rate constants of hDASPO compared to homologous enzymes (obtained at 25 °C).

	hDASPO	bDASPO (57)	hDAAO (31)
Substrate:	D-Asp	D-Asp	D-Ala
EMTN method:			
double reciprocal plot	convergent	Convergent	Parallel
k_{cat} (s^{-1})	229 ± 27	43.5	14.7
$K_{\text{m,D-AA}}$ (mM)	7.2 ± 1.2	1.6	8.2
$K_{\text{m,O}_2}$ (mM)	0.34 ± 0.11	0.46	1.2
RHR:			
k_{red} (s^{-1}), k_2	1550 ± 206 (460 at 10 °C)	180*	180
$K_{\text{d,app}}$ (mM)	23.7 ± 4.9	40	12.7
OHR ($\text{M}^{-1} \text{s}^{-1}$):			
Free reduced, k_4	$10.4 \pm 0.6 \times 10^4$	5.3×10^2 ^a	1.7×10^4
Meso-tartrate complex	$9.8 \pm 0.7 \times 10^4$	n.d.	n.d.
Oxaloacetate complex	$11.5 \pm 1.0 \times 10^4$		
Iminoaspartate(oxaloacetate and ammonia) complex, k_5	$\sim 15 \times 10^4$	1.5×10^4	1.3×10^5

^a determined at 4 °C; n.d., not determined

Structure and kinetic properties of human D-aspartate oxidase, the enzyme controlling D-aspartate levels in brain

Gianluca Molla, Antonio Chaves-Sanjuan, Antonio Savinelli, Marco Nardini, Loredano Pollegioni

Marco Nardini, Email: marco.nardini@unimi.it

Loredano Pollegioni, Email: loredano.pollegioni@uninsubria.it

Supplementary Table 1. Data collection and refinement statistics.

Data set	hDASPO (C141Y/C143G)
Data Collection	
Space Group	C222 ₁
Cell dimensions	
a, b, c (Å)	114.40, 159.72, 288.58
α , β , γ (°)	90.0, 90.0, 90.0
Wavelength (Å)	0.97949
Resolution range (Å)	
upper limit along a*, b*, c*	4.72, 3.94, 3.21 (3.66-3.22) [‡]
lower limit	144.29
#R _p im	0.133 (0.518) [‡]
+CC1/2	0.986 (0.535) [‡]
<I/ σ (I)>	5.9 (1.6) [‡]
Redundancy	5.8 (5.5) [‡]
Completeness (%)	
spherical	53.5 (8.7)
ellipsoidal	92.7 (72.4)
Wilson B-factor along a*, b*, c*	201.91, 115.10, 41.02
Refinement	
Resolution (Å)	93.00-3.22 (3.34 -3.22)
Number of reflections	23110 (114)
R _{work} /R _{free}	0.231/0.272 (0.381/0.483)
Number of molecules	
Proteins in the AU	6
FAD molecules	6
Glycerol molecules	6
Tris molecules	3
Phosphate molecules	2
Water molecules	179

Average B factors (Å ²)	53.93
Rmsd bond lengths (Å)	0.004
Rmsd bond angles (°)	0.73
Ramachandran plot statistics	93.32 % in favoured
	0.00 % outliers
Highest-resolution shell is shown in parentheses	
‡Anisotropically truncated data	
$^{\#}R_{p.i.m.} = \frac{1}{n} \sqrt{\frac{1}{n} \sum_{j=1}^n I_{hkl} - \langle I_{hkl} \rangle ^2} / I_{hkl,j}$	
†CC1/2 is the correlation coefficient of the mean intensities between two random half-sets of data.	

Supplementary Table 2. Comparison of apparent steady state parameters of hDASPO on different substrates.

Substrate	$k_{cat,app}$ (s^{-1})	$K_{m,app}$ (mM)	$k_{cat,app}/K_{m,app}$ ($mM^{-1}s^{-1}$)
D-Asp	81.3 ± 1.5	1.05 ± 0.06	77.4 ± 2.0
NMDA	73.6 ± 1.3	2.76 ± 0.12	26.7 ± 0.8
D-Glu	11.3 ± 0.3	31.5 ± 2.0	0.36 ± 0.02
D-Asn	8.3 ± 0.2	67.0 ± 4.1	0.12 ± 0.01
D-His	1.2 ± 0.1	96 ± 15	0.011 ± 0.001
D-Pro	1.2 ± 0.1	339 ± 65	0.003 ± 0.001

Supplementary Table 3. Expression level, thermal stability and apparent kinetic (on D-Asp at 21% oxygen saturation) of hDASPO variants.

Variants	Expression levels (purified protein)		Specific activity	Thermal stability	Apparent kinetic parameters		
	(U/L _{fermentation})	(mg _{prot} /L _{fermentation})	(U/mg)	T _m (°C)	K _{m,app} (mM)	k _{cat,app} (s ⁻¹)	k _{cat,app} /K _m (mM ⁻¹ s ⁻¹)
Wild-type	2855	29.9	95.5	48.8	1.1 ± 0.1	81.3 ± 1.5	77.4 ± 2.0
C269S	1313	12.7	103.2	53.1	1.3 ± 0.1	85.9 ± 2.1	68.2 ± 1.7
C328S	804	9.6	83.3	53.1	1.0 ± 0.1	68.9 ± 1.9	68.2 ± 1.9
C328V	493	7.8	63.9	51.6	1.0 ± 0.1	80.6 ± 2.6	82.2 ± 2.6
C141SC143S	77	0.9	81.7	40.9	1.6 ± 0.3	32.8 ± 1.4	20.5 ± 0.9
C141Y/C143G (hDASPO*)	311	3.8	81.4	48.1	1.3 ± 0.1	68.6 ± 1.9	53.1 ± 1.5
C269S/C328S	518	7.0	74.5	53.5	2.5 ± 0.3	69.7 ± 2.1	28.0 ± 1.1
C141Y/C143G/C328S	164	1.1	153.8	52.8	1.2 ± 0.2	72.9 ± 2.9	59.3 ± 2.3
C29S/C269S/C328S	646	6.2	104.3	45.0	1.8 ± 0.5	69.9 ± 5.6	39.7 ± 1.6

Supplementary Table 4. Comparison of apparent steady state parameters of wild-type, H54A and R237A hDASPO variants on selected D-amino acids.

Enzyme form	$k_{cat,app}$ (s^{-1})	$K_{m,app}$ (mM)	$k_{cat,app}/K_{m,app}$ ($mM^{-1}s^{-1}$)
D-Aspartate:			
Wild-type	81.3 ± 1.5	1.05 ± 0.06	77.4 ± 2.0
H54A	65.2 ± 0.1	1.45 ± 0.04	45.0 ± 0.9
R237A	55.7 ± 1.3	22.2 ± 2.1	2.5 ± 0.3
NMDA:			
Wild-type	73.2 ± 0.9	2.75 ± 0.10	26.6 ± 0.8
H54A	114.0 ± 2.9	1.89 ± 0.2	60.3 ± 6.6
R237A	65.5 ± 1.8	11.3 ± 1.1	5.8 ± 0.6
D-Glutamate:			
Wild-type	11.3 ± 0.3	31.5 ± 2.0	0.36 ± 0.02
H54A	11.2 ± 0.2	59.4 ± 4.5	0.19 ± 0.02
R237A	9.8 ± 0.2	43.3 ± 5.9	0.23 ± 0.02
D-Asparagine:			
Wild-type	8.3 ± 0.2	67.0 ± 4.1	0.12 ± 0.01
H54A	29.1 ± 3.2	≥ 250	≤ 0.12
R237A	11.2 ± 0.2	59.0 ± 4.5	0.19 ± 0.02

Figure 1

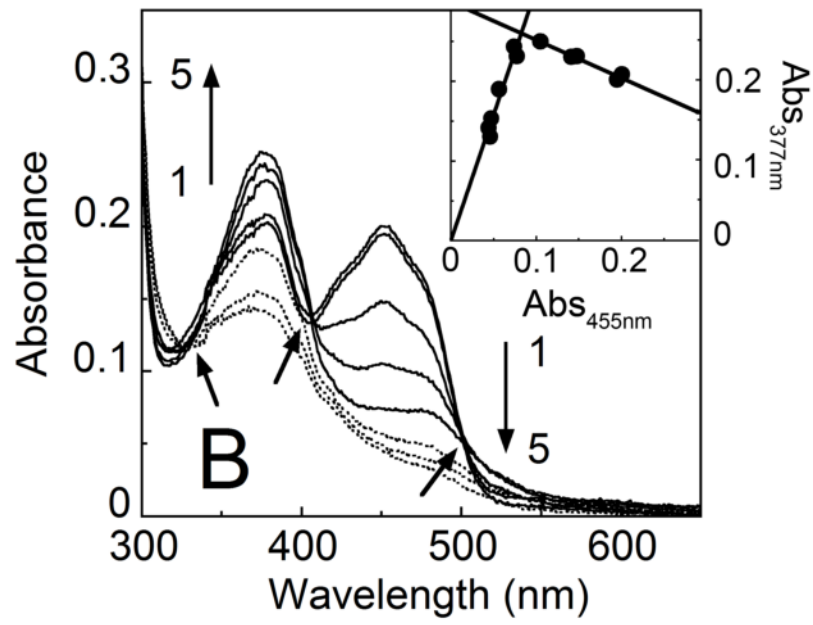
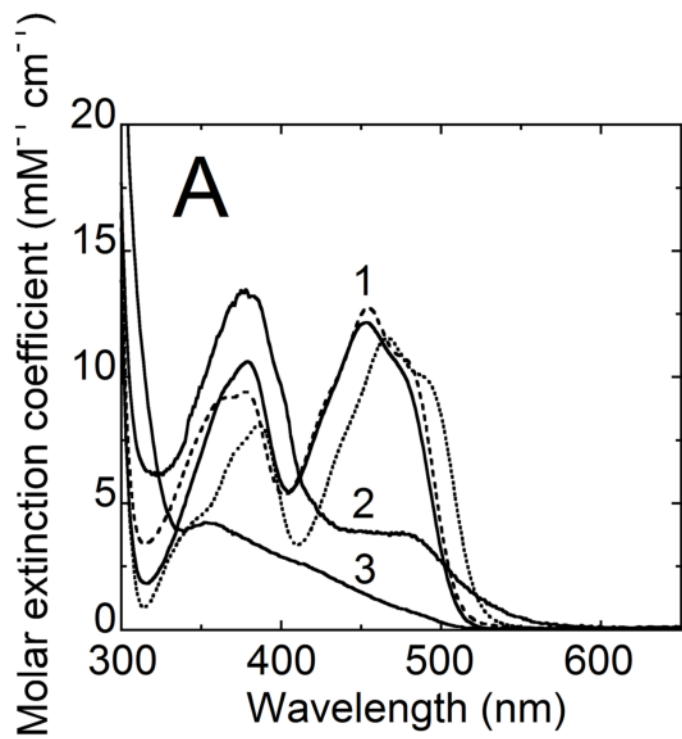


Figure 2

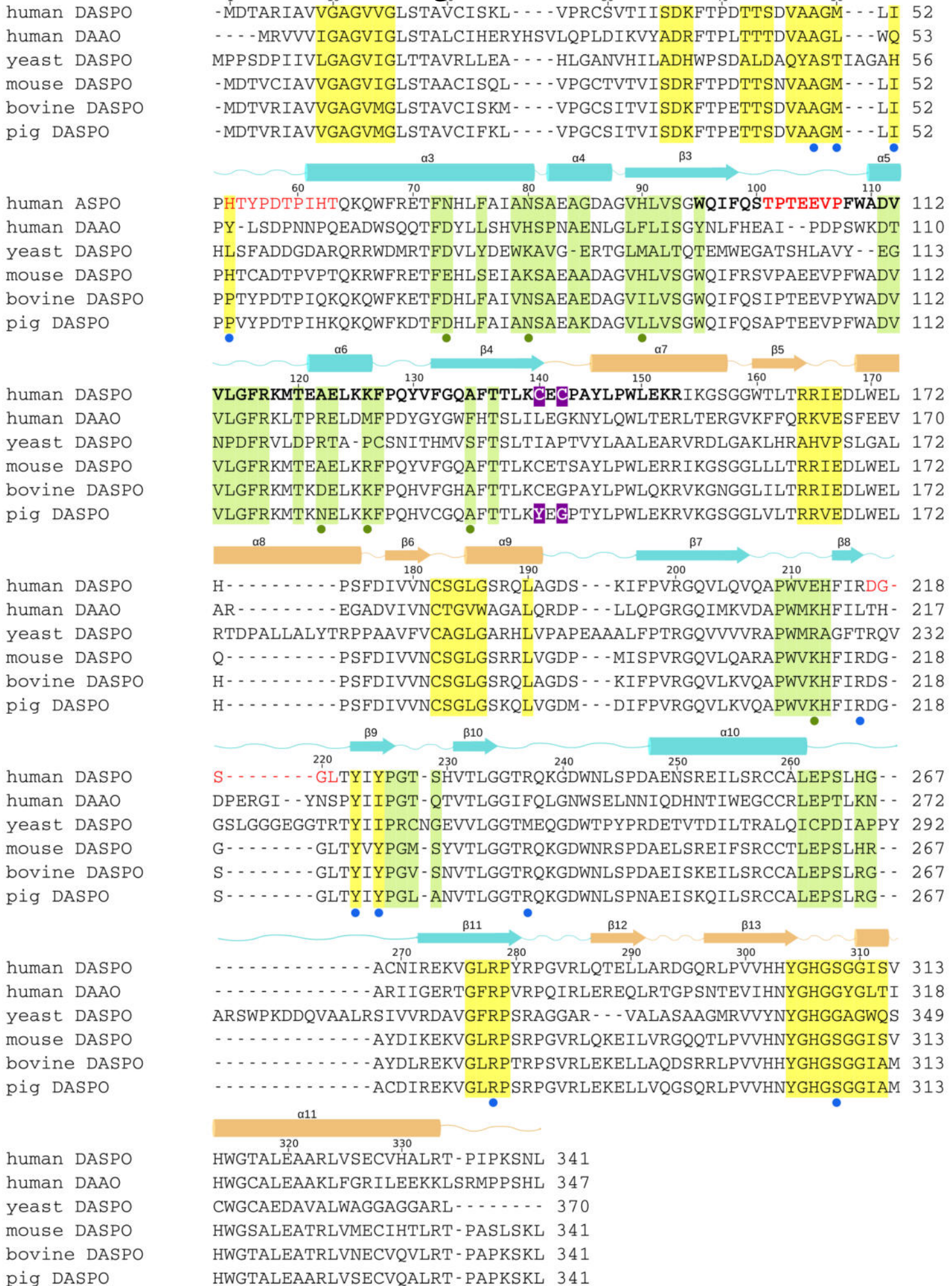


Figure 3

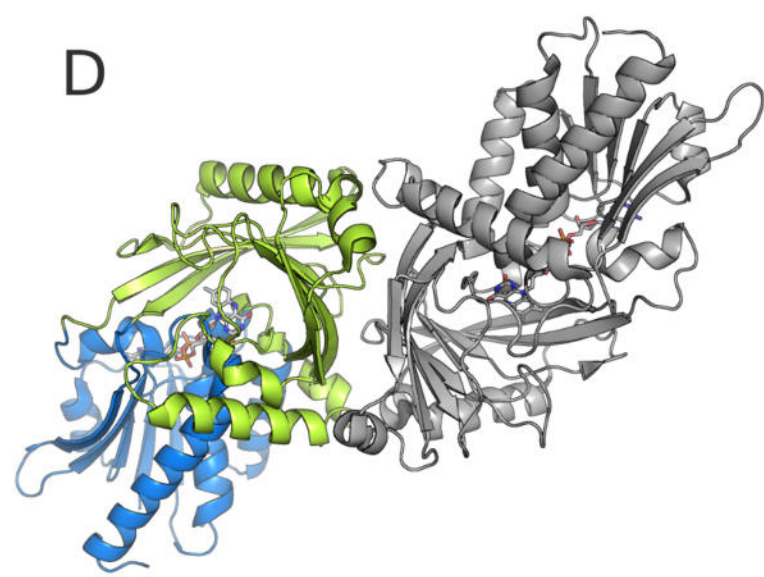
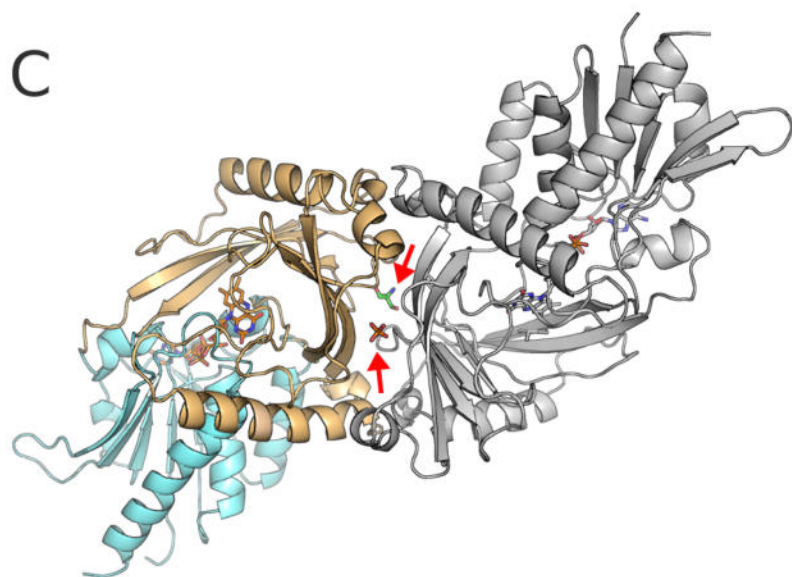
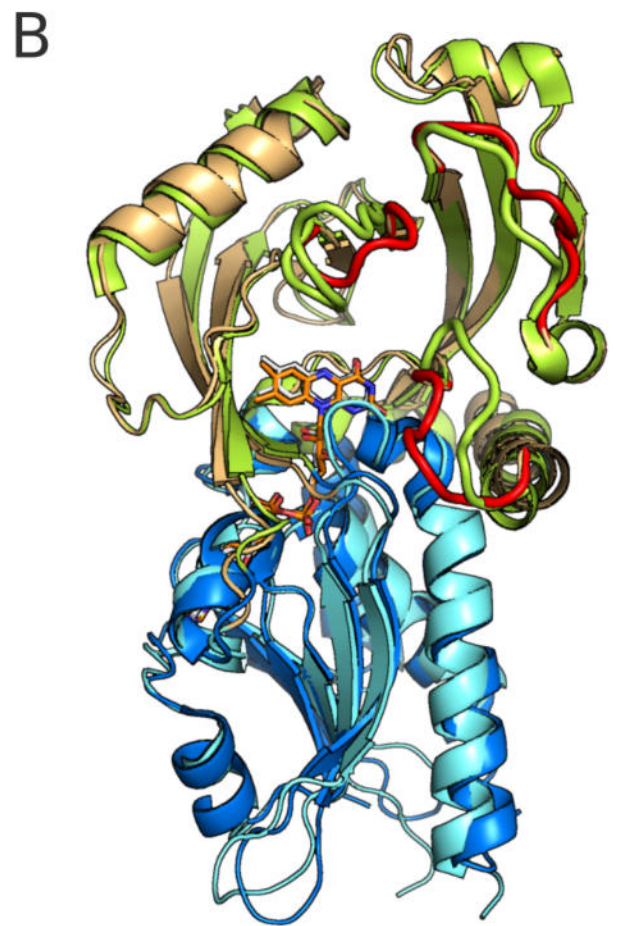
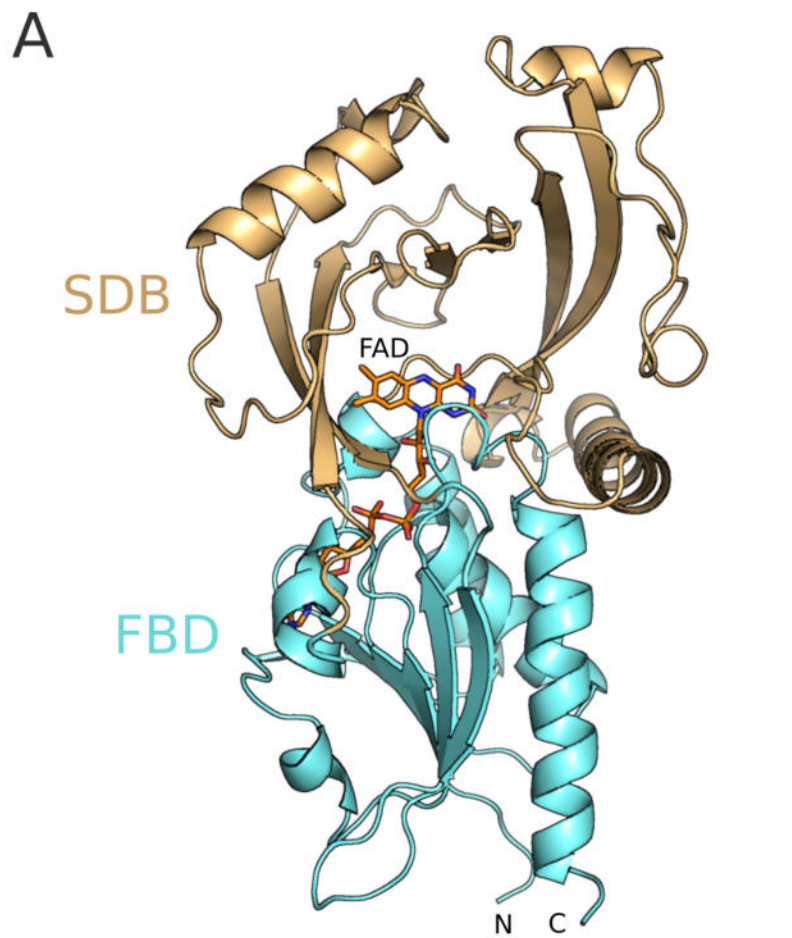


Figure 4

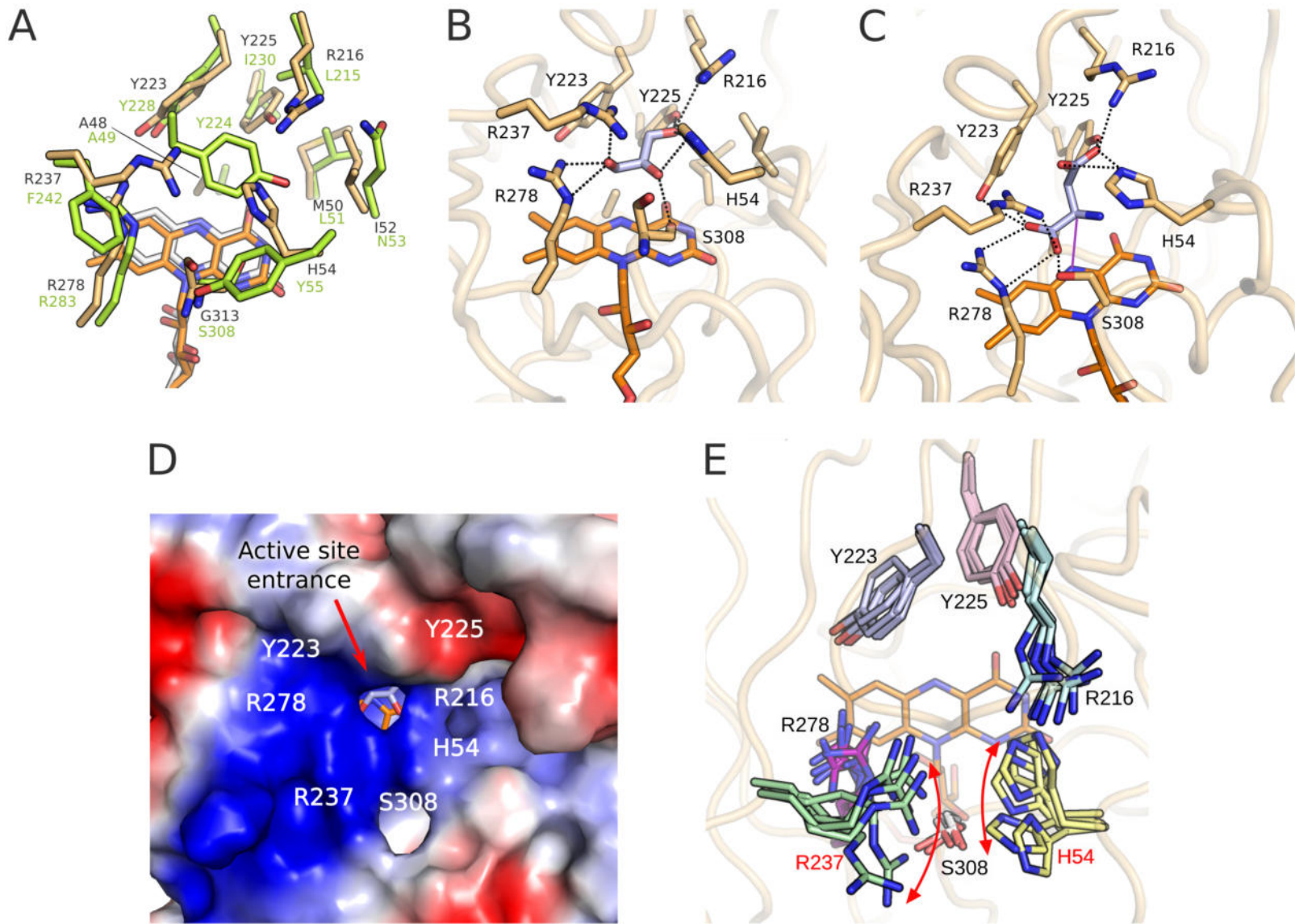


Figure 5

Extinction molar coefficient ($\text{mM}^{-1} \text{cm}^{-1}$)

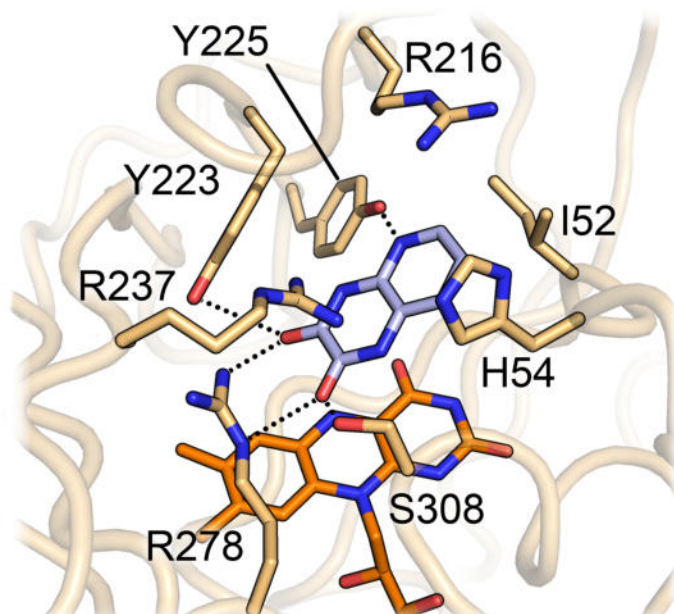
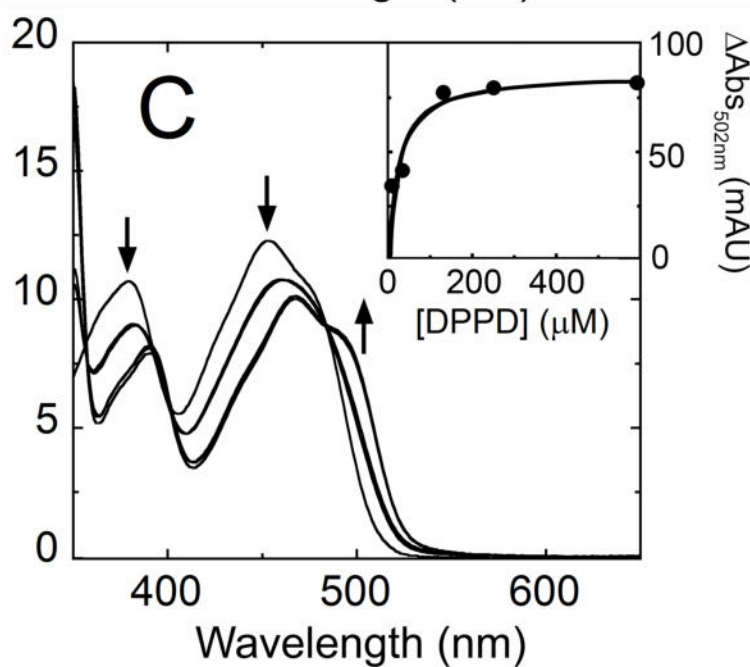
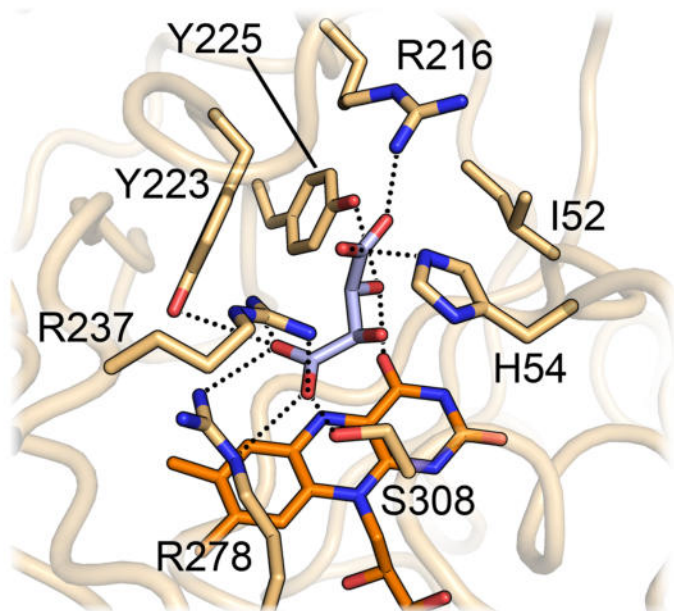
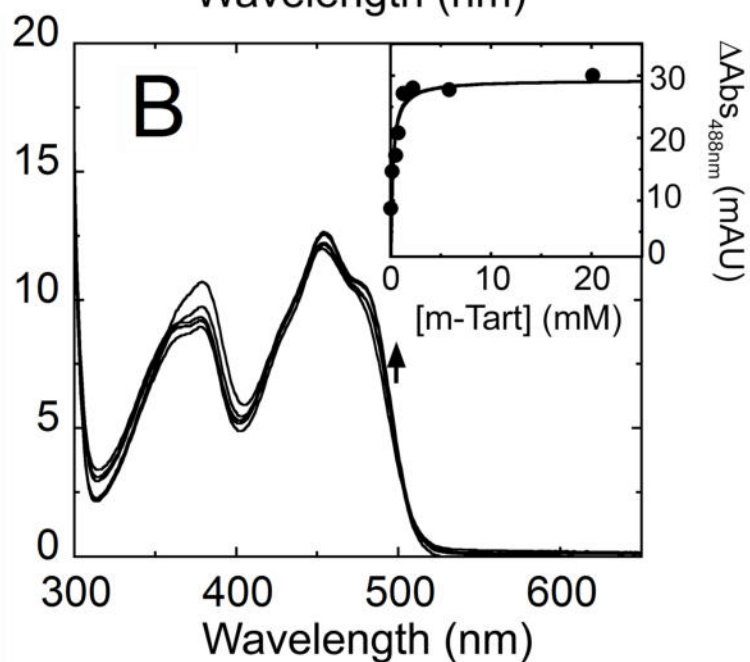
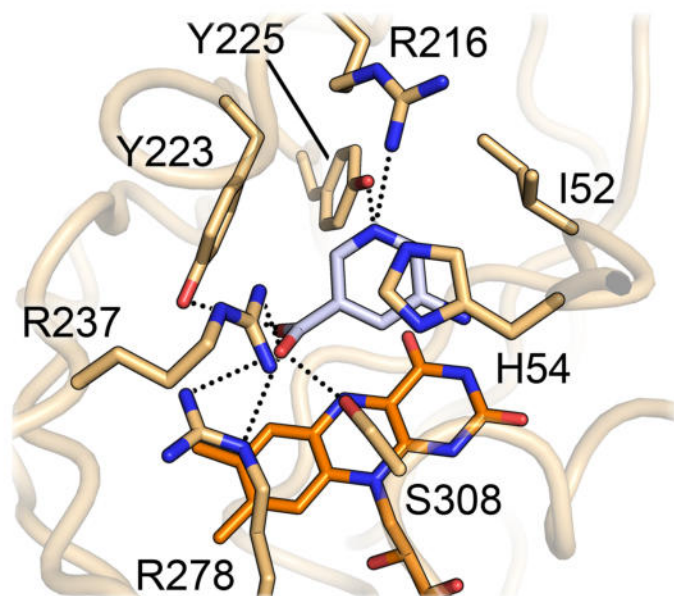
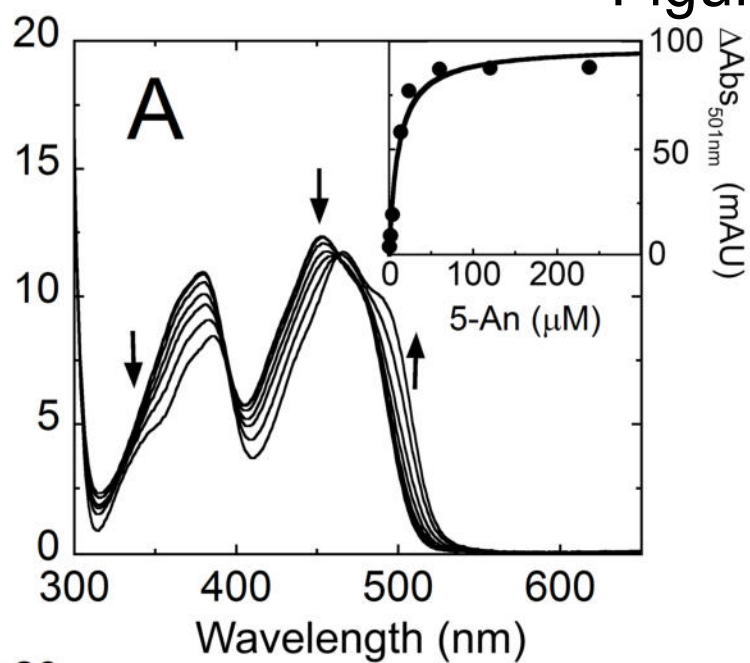
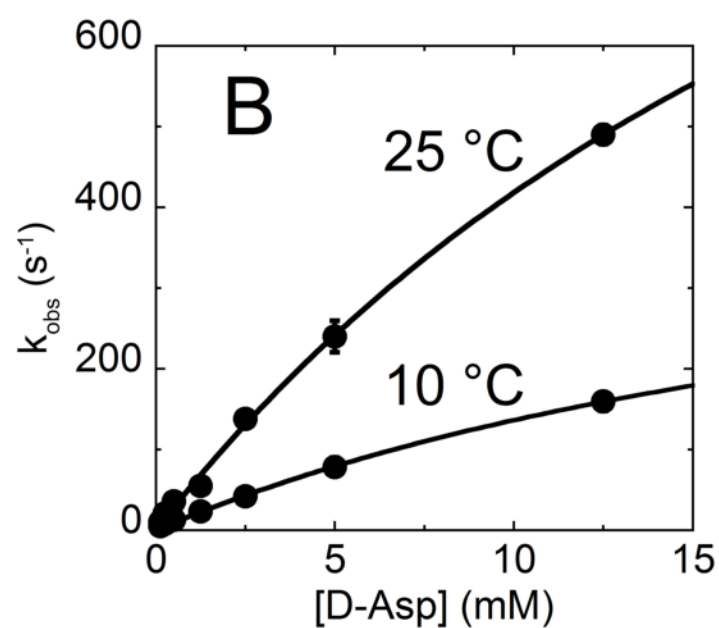
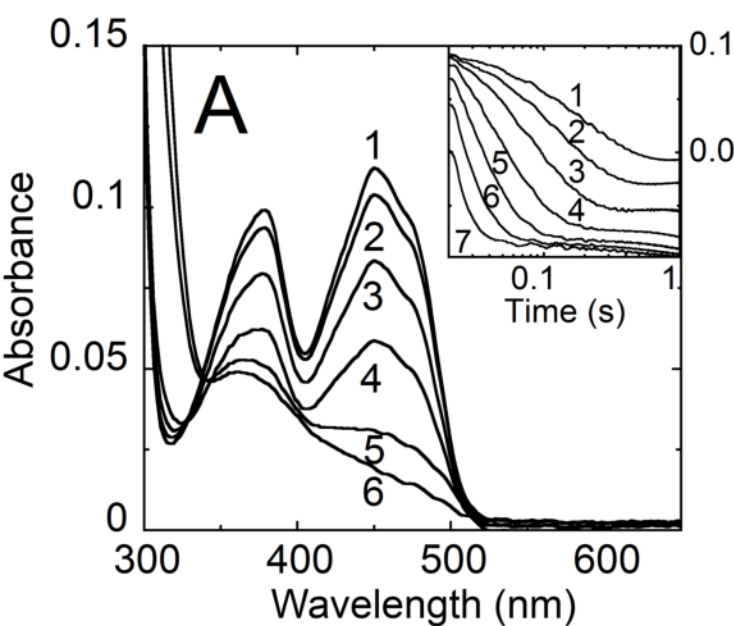
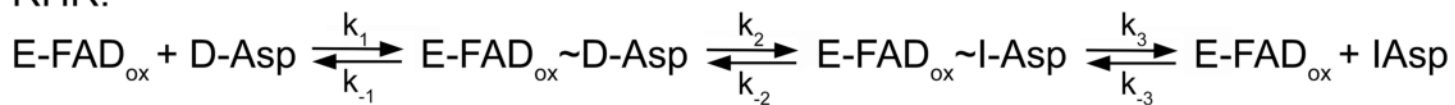
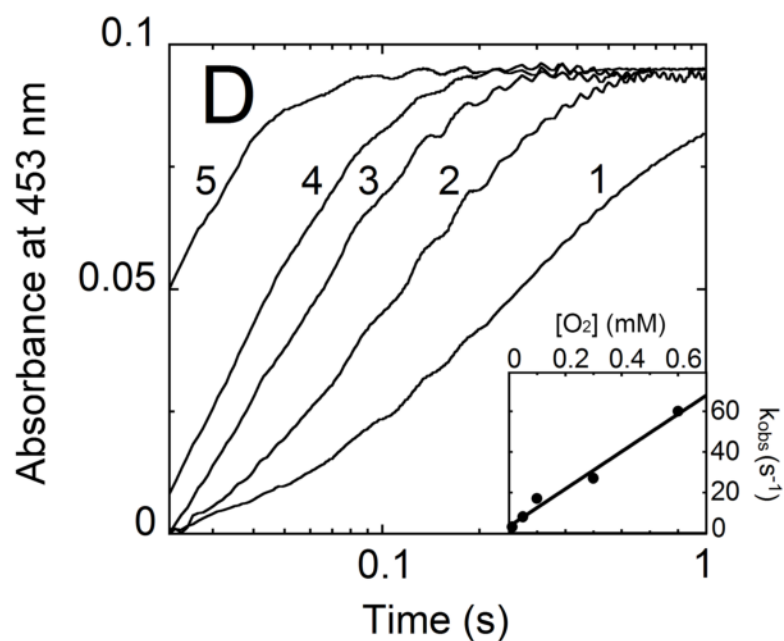
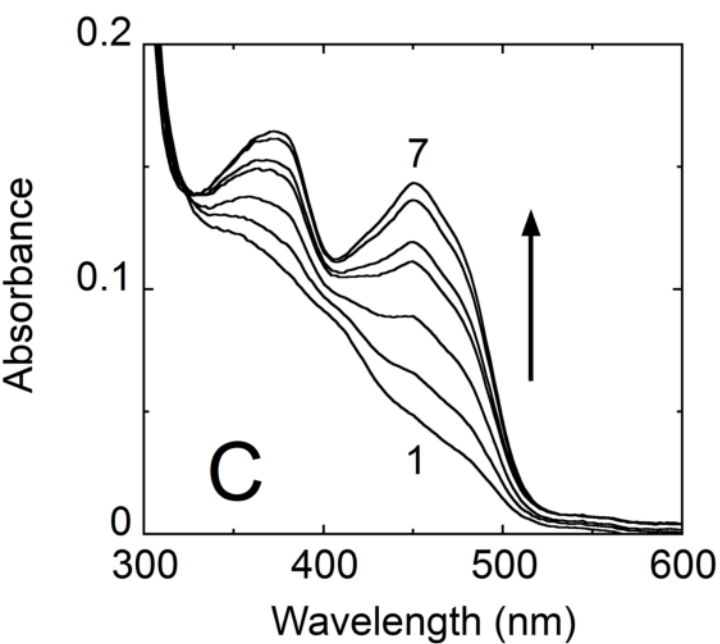
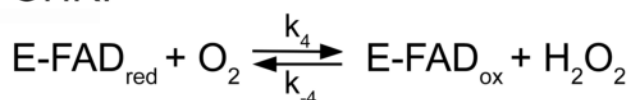


Figure 6

RHR:



OHR:



Structure and kinetic properties of human D-aspartate oxidase, the enzyme controlling D-aspartate levels in brain

Gianluca Molla, Antonio Chaves-Sanjuan, Antonio Savinelli, Marco Nardini, Loredano Pollegioni

Marco Nardini, Email: marco.nardini@unimi.it

Loredano Pollegioni, Email: loredano.pollegioni@uninsubria.it

Supplementary Data 1. Protein purification and spectral properties

H54A and R237A hDASPO variants were generated by site-directed mutagenesis using the QuikChange Lightning Site-Directed Mutagenesis kit (Agilent) and the following primers: H54A: primer up: 5'-GCCGGAATGCTTATTCCTGCCACTTATCCAGATACACCG-3', primer down: 5'-CGGTGTATCTGGATAAGGCTGAGGAATAAGCATTCCGGC-3'; R237A: primer up: 5'-ACCCTGGGTGGAAGCTCAAAAAGGGGACTGG-3', primer down: 5'-CCAGTCCCCTTTTGGAGCAGTCCACCCAGGGT-3'.

Recombinant hDASPO (both the wild-type and the variants) was purified from the crude extract of *E. coli* BL21(DE3) LOBSTR cells bearing the pET11-His-hDASPO plasmid, grown under optimized conditions (i.e. collecting the cells 18 h after adding 10 μ M IPTG at an $OD_{600nm} \approx 0.5$). SDS-PAGE analysis of the whole cells showed the appearance of a band at ≈ 39 kDa corresponding to hDASPO following IPTG addition, with the highest productivity at 18 h from the inducer addition (representing $\approx 4\%$ of the protein content for wild-type DASPO) (see Supplementary Fig. 1, lane 3). A comparison between the amount of hDASPO in the crude extract and in the insoluble fraction of the cell lysate (based on densitometry analysis) shows that more than 90% of the recombinant enzyme was expressed as a soluble protein (Supplementary Fig. 1, lanes 5 and 6). A single chromatographic step on a HiTrap chelating column allowed the purification of 29.9 mg of wild-type hDASPO/liter of fermentation broth – a value significantly higher than those previously reported (≈ 2 -3 mg/liter) [1-3]. A higher degree of homogeneity was apparent eluting bound hDASPO at 250

mM than at 500 mM imidazole, see lanes 9 and 10 in Supplementary Fig. 1: a purity > 95% was obtained, as judged by SDS-PAGE analysis. The purification yield of recombinant H54A and R237A hDASPO variants was 18 and 31.1 mg/liter.

The purified wild-type hDASPO shows the canonical absorbance spectrum of FAD-containing flavoproteins with three main peaks at 273, 379, and 453 nm (Fig. 1A). The ratio between the absorbance at 273 and 453 nm is 10.4, and the estimated molar extinction coefficient is 12,185 M⁻¹ cm⁻¹ at 454 nm (Fig. 1A). The oxidized form of hDASPO is fully converted into the reduced state by adding a > 2-fold molar excess of D-Asp under anaerobic conditions (Fig. 1A). hDASPO is photoreduced in the presence of 5 mM EDTA and 60 nM 5-deazaflavin at 4 °C and pH 8.0 forming a red anionic semiquinone: three isosbestic points were observed during the semiquinone formation (at 345, 407, and 502 nm, Fig. 1B) pointing to the presence of only two forms, i.e. the oxidized and semiquinone species. A high amount of semiquinone form is stabilized by hDASPO (≈ 78%). At > 6 minutes of irradiation, the amount of semiquinone species decreased and a complete reduced form was observed after 16 minutes (Fig. 1B, dotted lines and inset). A complete re-oxidation of the cofactor was observed when the enzyme was kept in the dark for 16 hours under anaerobic conditions, even in the absence of a mediator such as benzyl viologen. This result points to a kinetic stabilization of the anionic flavin semiquinone, as observed with other flavoenzymes [4].

1. C. Setoyama, R. Miura, Structural and functional characterization of the human brain D-aspartate oxidase. *J. Biochem.* **121**, 798-803 (1997).
2. M. Katane, et al., Characterization of the enzymatic and structural properties of human D-aspartate oxidase and comparison with those of the rat and mouse enzymes. *Biol. Pharm. Bull.* **38**, 298-305 (2013).
3. M. Katane, et al., Identification of novel D-aspartate oxidase inhibitors by *in silico* screening and their functional and structural characterization *in vitro*. *J. Med. Chem.* **58**, 7328-7340 (2015).
4. V. Massey, P. Hemmerich, Active-site probes of flavoproteins. *Biochem. Soc. Trans.* **8**, 246-357 (1980).

Structure and kinetic properties of human D-aspartate oxidase, the enzyme controlling D-aspartate levels in brain

Gianluca Molla, Antonio Chaves-Sanjuan, Antonio Savinelli, Marco Nardini, Loredano Pollegioni

Marco Nardini, Email: marco.nardini@unimi.it

Loredano Pollegioni, Email: loredano.pollegioni@uninsubria.it

Supplementary Data 2. Selection of cysteine residues to generate hDASPO variants for protein crystallization

A model of hDASPO three dimensional structure has been generated using the I-TASSER (<http://zhanglab.ccmb.med.umich.edu/I-TASSER/>) and SwissModel (<http://swissmodel.expasy.org/>) servers and the structure of hDAAO as template (PDB 3g3e, 39% sequence identity). The quality of the model has been validated by SAVES metaserver and six different programs, such as PROVE and ERRAT (<https://services.mbi.ucla.edu/SAVES/>) [5].

The conservation analysis by the ConSurf server (<http://consurf.tau.ac.il>) shows that among the nine cysteine residues present in hDASPO, five are not conserved in hDAAO (namely C29, C141, C143, C269 and C328) and two of these are not conserved in pig DASPO (C141 and C143, Fig. 2). Three cysteines are solvent exposed in the model (C29, C269 and C328) thus putatively prompted to generate interchain disulfide bonds. Only C182 and C258 are internal residues conserved in all the hDASPO homologues.

Based on these analyses, cysteines at positions 29, 269 and 328 (on the protein surface) and 141 and 143 (not conserved in pig DASPO and hDAAO) have been selected for mutagenesis. Cysteines 29, 269 and 328 were substituted to serine; cysteines 141 and 143 were substituted in tyrosine and glycine (to resemble the sequence of pig DASPO); cysteine 328 in valine as in pig DAAO.

The hDASPO C269S, C328S and C328V single point variants, the C269S/C328S, C141S/C143S and C141Y/C143G double point variants, and the C29S/C269S/C328S and C141Y/C143G/C328S triple

variants have been generated by site directed mutagenesis using the Quick Change II XL kit (Agilent). The expression level and specific activity on D-Asp of the purified hDASPO variants is reported in Supplementary Table 1: the lowest expression yield was obtained for the C141S/C143S and C141Y/C143G/C328S variants (~ 1 mg enzyme/L fermentation). All hDASPO variants were purified as holoenzymes. The apparent kinetic parameters on D-Asp and thermal stability (estimated by temperature ramp experiments) demonstrate that all variants are active: only for the C141S/C143S a ~ 8 °C lower T_m and a 2.5-fold lower $k_{cat,app}$ was apparent. This hDASPO variant also slightly differs in the far-UV CD spectrum.

All hDASPO variants purified to a high degree of homogeneity (see lane 10 in Supplementary Fig. 1) have been tested in preliminary crystallization trials, with only the C141Y/C143G variant (named hDASPO*) providing well diffracting crystals.

5. J. Pontius, J. Richelle, S.J. Wodak, Deviations from standard atomic volumes as a quality measure for protein crystal structures. *J. Mol. Biol.* **264**, 121-136 (1996).

Structure and kinetic properties of human D-aspartate oxidase, the enzyme controlling D-aspartate levels in brain

Gianluca Molla, Antonio Chaves-Sanjuan, Antonio Savinelli, Marco Nardini, Loredano Pollegioni

Marco Nardini, Email: marco.nardini@unimi.it

Loredano Pollegioni, Email: loredano.pollegioni@uninsubria.it

Supplementary Data 3. hDASPO holoenzyme reconstitution

The kinetics of the holoenzyme reconstitution was studied under pseudo-first-order conditions (5- to 50-fold excess of FAD) by following the quenching of protein fluorescence. The reaction was biphasic. In the first rapid phase (approx. 30-40 s) the quenching in protein fluorescence represented ~20-40% of the total change and the rate was proportional to the FAD concentration (Supplementary Fig. 6B): a $k = 9.6 \times 10^5 \text{ M}^{-1}\text{s}^{-1}$ was calculated. On the other hand, the changes in protein fluorescence related to the slower, second phase did not depend on the FAD concentration, $k = 0.13 \text{ s}^{-1}$. Considering the appearance of the catalytic activity (by the polarographic method) after the FAD injection (20-fold molar excess), the oxygen consumption rapidly increased reaching the maximal activity (100 U/mg) in 30-40 s, consistently to the completion of the first phase observed following protein fluorescence changes.

Structure and kinetic properties of human D-aspartate oxidase, the enzyme controlling D-aspartate levels in brain

Gianluca Molla, Antonio Chaves-Sanjuan, Antonio Savinelli, Marco Nardini, Loredano Pollegioni

Marco Nardini, Email: marco.nardini@unimi.it

Loredano Pollegioni, Email: loredano.pollegioni@uninsubria.it

Supplementary Data 4. Kinetic mechanism of hDASPO

Steady-state kinetics. In EMTN, the oxidized enzyme, 6.1 μM , was mixed aerobically with increasing amounts of D-Asp (0.5 - 5 mM) and the changes in flavin absorption monitored at 450 nm. A very rapid decrease in absorbance during the first 100 ms was observed, accounting to 55-60% of the total change and corresponding to a flavin reduction reaction, followed by an increase of absorbance up to 0.2-2 s (which intensity depended on the initial D-Asp concentration); then the reaction entered into a steady state phase which lead to the fully reduced enzyme (Supplementary Fig. 8). The 450 nm traces were analyzed as function of oxygen concentration (the limiting substrate) according to [6]. The double reciprocal plot in the inset of Supplementary Fig. 8 shows a set of lines converging on the negative abscissa: this is compatible with formation of a ternary complex mechanism [7]. Using the Dalziel approach, the k_{cat} and K_{m} values for D-Asp and O_2 were calculated (Table 2). While the K_{m,O_2} is very similar to the value for bovine DASPO, the $K_{\text{m},\text{D-Asp}}$ and k_{cat} values are ~5-fold higher, suggesting a different rate limiting step in catalysis.

Reductive half-reaction. The reductive half-reaction was studied at 10 and 25 °C. For these experiments, 21.9 μM hDASPO was anaerobically mixed with increasing concentrations of D-Asp (0.125-12.5 mM). The absorbance change at 450 nm is biphasic, both at 10 °C and 25 °C (Fig. 6A,B): the first, rapid phase was interpolated with a single exponential curve. A full flavin reduction is only apparent at D-Asp concentration ≥ 2.5 mM, suggesting that the reductive half-reaction is reversible. This was confirmed by static anaerobic titration of reduced enzyme with oxaloacetate (OA) in the presence of 8.5 mM ammonium chloride to generate the product iminoaspartate (IAsp): FAD is

reoxidized adding OA and newly reduced adding further D-Asp (Supplementary Fig. 9). Assuming that all OA is converted into IAsp, an equilibrium constant of 4.7 ± 1.3 was estimated for the overall $E_{ox} + D\text{-Asp} \leftrightarrow E_{red} + I\text{Asp}$ process. Adding OA to the reduced hDASPO in the absence of ammonium chloride does not allow flavin reduction.

The second, slow phase of absorbance change at 450 nm was insensitive to D-Asp concentration and tends to disappear at high D-Asp concentration. The step of IAsp release from the reduced E-FAD_{red}-IAsp complex is not evident in stopped-flow experiments (k_3 in the scheme in Fig. 6top).

A direct plot of the observed rates for the reduction of the first phase, k_{obs1} , at increasing D-Asp concentration shows an hyperbolic behavior (Fig. 6B), that describes a first-order reaction of a binary complex (k_2/k_{-2}) that follows a second-order complex formation (k_1/k_{-1}), according to [8]. The step of binding (k_1 and k_{-1}) is not observed spectrophotometrically. The linearity of double reciprocal plot (not shown) is compatible with a situation in which k_2 is $> k_{-2}$ (see the scheme in Fig. 6top).

From the direct plot reported in Fig. 6B, a k_{red} (k_2) of 1553 s^{-1} and 460 s^{-1} was estimated (at $25 \text{ }^\circ\text{C}$ and $10 \text{ }^\circ\text{C}$, respectively), a value 10-fold higher than the k_{cat} value, indicating that this step is not rate limiting in catalysis.

Oxidative half-reaction. For the oxidative half-reaction $24.4 \text{ } \mu\text{M}$ hDASPO was reduced by adding a 4-fold molar excess of D-Asp under anaerobic conditions, in the absence (from the E-FAD_{red} form, Fig. 6C,D) or in the presence of 3.35 mM meso-tartrate (MT, Supplementary Fig. 10, from the E-FAD_{red}-ligand form). The reduced enzyme was then mixed in the stopped-flow instrument with a buffer containing increasing oxygen concentrations, at $25 \text{ }^\circ\text{C}$. In both cases, an increase in the 453 nm absorbance was observed that was satisfactorily fitted with a single exponential process: a reoxidation rate constant (k_4 or k_{reox}) of $10.4 \pm 0.6 \times 10^4 \text{ M}^{-1}\text{s}^{-1}$ for the free enzyme form and of $9.8 \pm 0.7 \times 10^4 \text{ M}^{-1}\text{s}^{-1}$ in the presence of MT, respectively, was determined, a figure significantly faster than the value reported for bovine DASPO ($0.053 \times 10^4 \text{ M}^{-1}\text{s}^{-1}$ at $4 \text{ }^\circ\text{C}$) [9].

In order to measure the rate of reoxidation of the reduced enzyme in complex with the product iminoacid (k_5 , see scheme on top of Supplementary Fig. 10), we mixed the reduced enzyme with 10 mM OA and 0.1 M ammonium chloride (final concentrations): because of the reversibility of the

reductive half-reaction, the reoxidized enzyme species was largely generated. The reaction with dioxygen of the residual, small amount of reduced enzyme that was not reoxidized following IAsp generation showed rates similar to those determined for the free or the MT complex (Table 2).

Previous studies on bovine DASPO employed OA to mimic the substrate bound species instead of D-Asp (to avoid enzyme turnover after being reoxidized) [9]. Using increasing concentrations of OA in the absence of ammonium chloride (from 5 μ M to 5 mM) the observed rate constant of reoxidation doubled at OA concentration > 0.5 mM with respect to the free enzyme form (~ 30 vs. 19 s^{-1}). The kinetics of reoxidation of the reduced enzyme added of 1 mM OA at increasing O_2 concentration yielded a k_{reox} of $11.5 \pm 0.1 \times 10^4 \text{ M}^{-1}\text{s}^{-1}$, slightly faster than the free reduced hDASPO (see Table 2). This result confirms that the reoxidation rate constant k_5 from the E-FAD_{red}-ligand (representing the complex of the reduced enzyme with IAsp or with a second molecule of D-Asp) is only slightly faster than that of the free reduced species, k_4 . Altogether, we do not have any evidence of the binding of a second molecule of D-Asp as well as of a related, rate-limiting, conformational change.

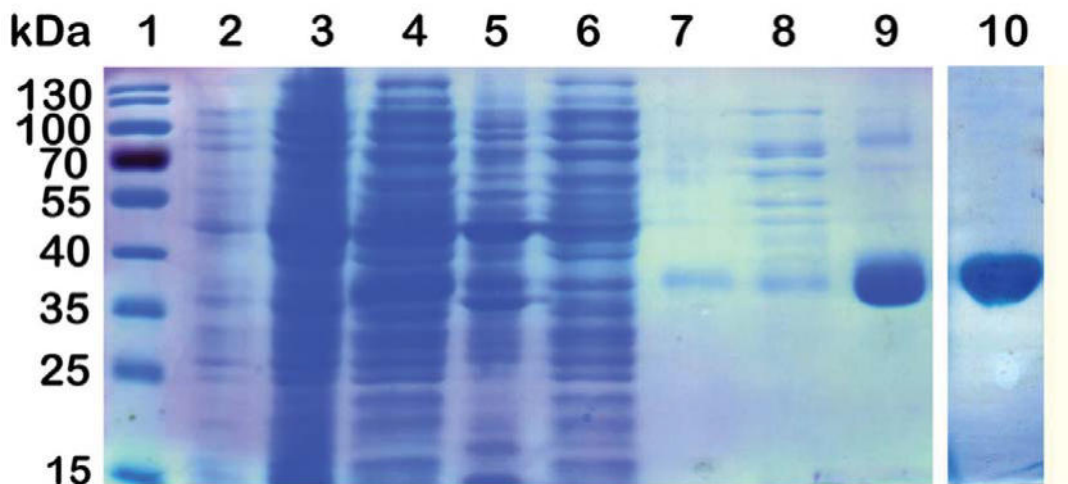
6. Q.H. Gibson, B.E. Swoboda, V. Massey, Kinetics and mechanism of action of glucose oxidase. *J. Biol. Chem.* **239**, 3927-3934 (1964).
7. K. Dalziel, The interpretation of kinetic data for enzyme-catalysed reactions involving three substrates. *Biochem. J.* **114**, 547-556 (1969).
8. S. Strickland, G. Palmer, V. Massey, Determination of dissociation constants and specific rate constants of enzyme-substrate (or protein-ligand) interactions from rapid reaction kinetic data. *J. Biol. Chem.* **250**, 4048-4052 (1975).
9. A. Negri, V. Massey, C.H. Williams, L.M. Schopfer, The kinetic mechanism of beef kidney D-aspartate oxidase. *J. Biol. Chem.* **263**, 13557-13563 (1988).

Structure and kinetic properties of human D-aspartate oxidase, the enzyme controlling D-aspartate levels in brain

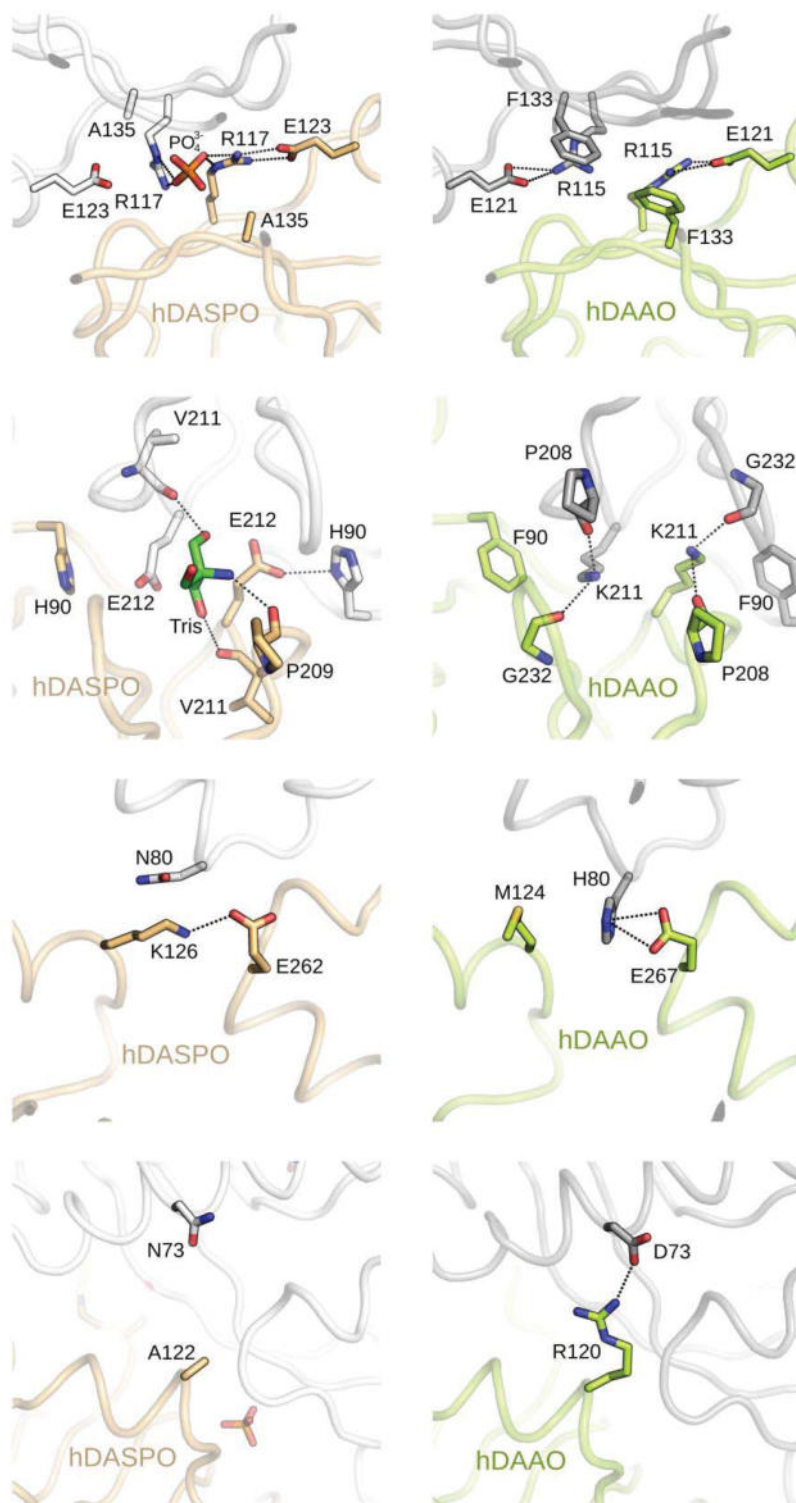
Gianluca Molla, Antonio Chaves-Sanjuan, Antonio Savinelli, Marco Nardini, Loredano Pollegioni

Marco Nardini, Email: marco.nardini@unimi.it

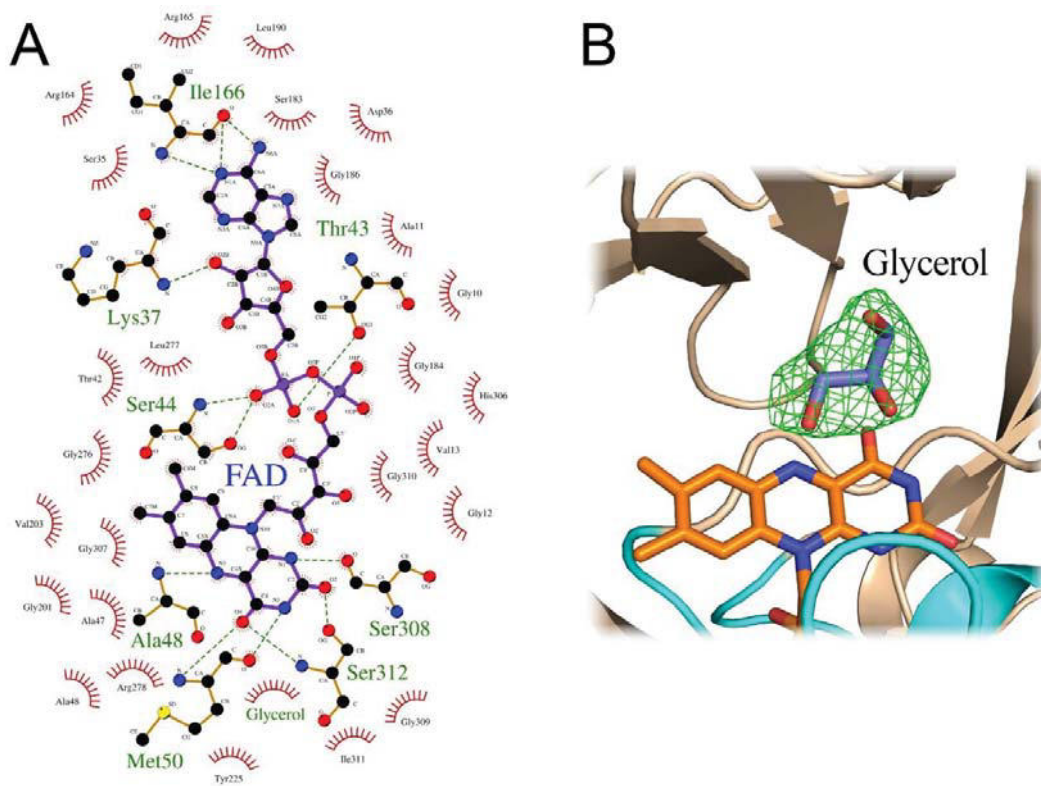
Loredano Pollegioni, Email: loredano.pollegioni@uninsubria.it



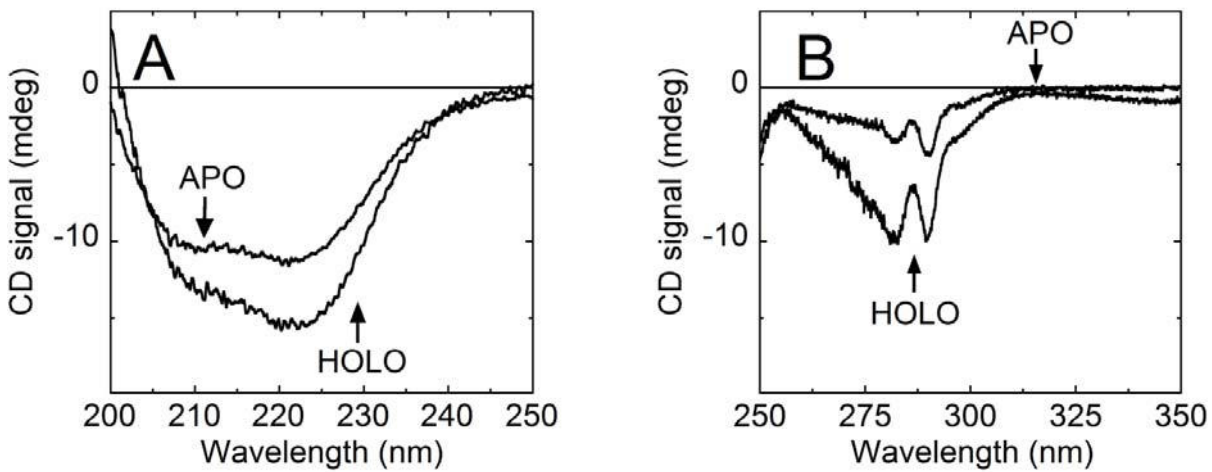
Supplementary Fig. 1. SDS-polyacrylamide gel electrophoresis of samples at various stages of hDASPO purification. Gel was stained with Coomassie blue. (1) Molecular-weight marker proteins; (2) whole cells before IPTG addition; (3) whole cells after 18 hours from IPTG addition; (4) crude extract (40 µg) and (5) insoluble fraction of cell lysate (40 µg); HiTrap chromatography flow-through (lane 6, 40 µg), proteins eluted at low imidazole concentration (lanes 7 and 8), and purified hDASPO eluted at 500 mM imidazole (lane 9, 10 µg: 93.7% purity); lane 10: hDASPO* eluted at 250 mM imidazole and used for biochemical and crystallization trials.



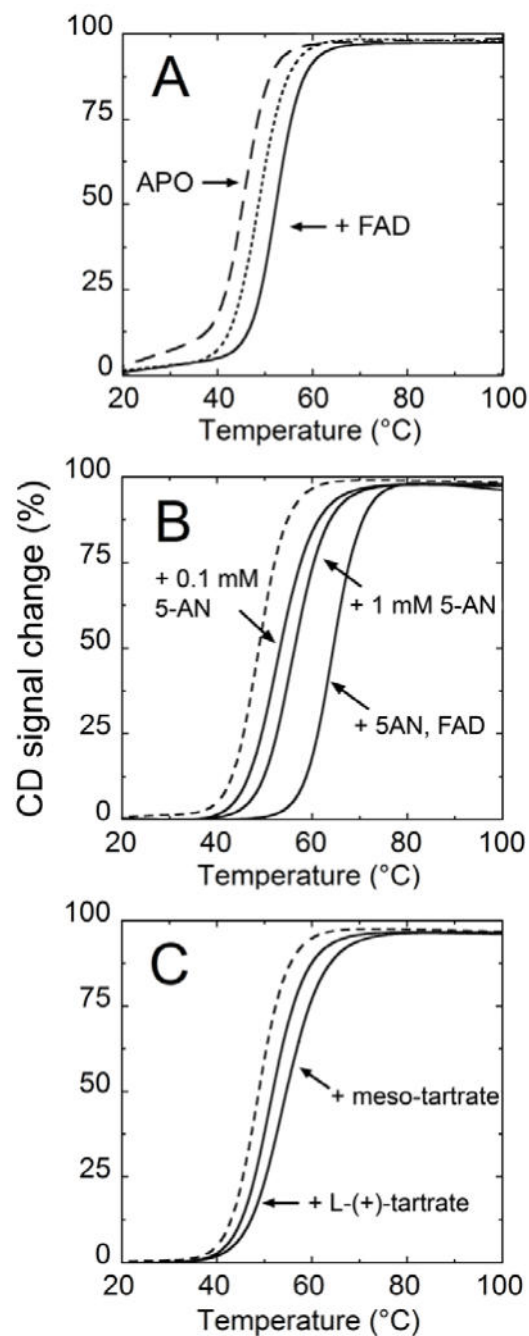
Supplementary Fig. 2. hDASPO* crystal packing vs hDAAO (dimer). hDASPO* and hDAAO are colored as in Fig. 2, with the subunit/protomer counterpart in gray. hDASPO* panels are on the left and hDAAO on the right, in the same orientation. Key residues for the monomer-monomer interaction are represented as sticks and the hydrogen bonds and salt bridges as dashed lines.



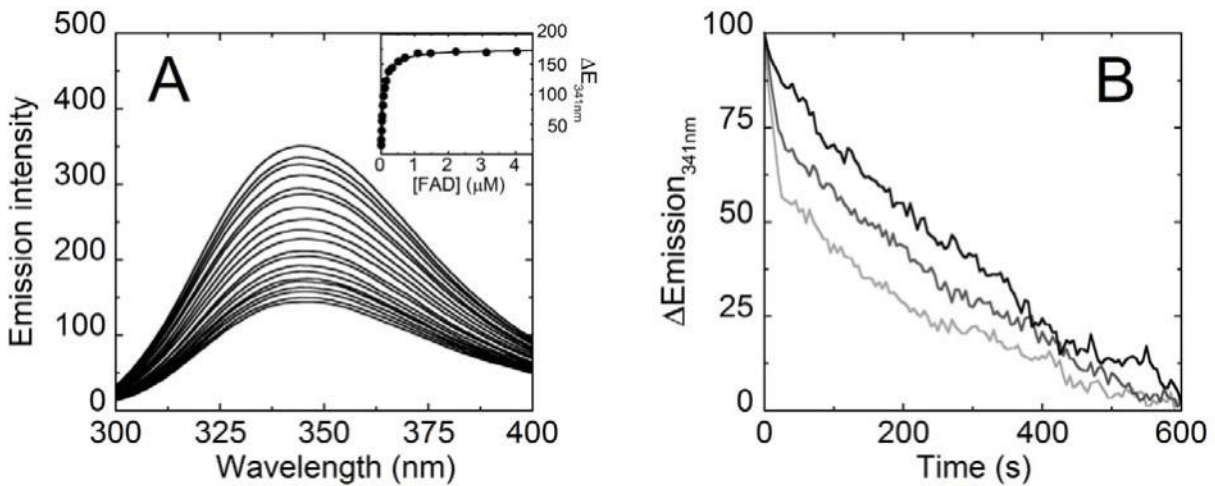
Supplementary Fig. 3. Details of hDASPO structure. A) hDASPO-FAD interactions. The figure was rendered using the program LIGPLOT. B) Electron density 2Fo-Fc map (green net, contoured at 1 σ) at the hDASPO* active site for the modeled glycerol molecule.



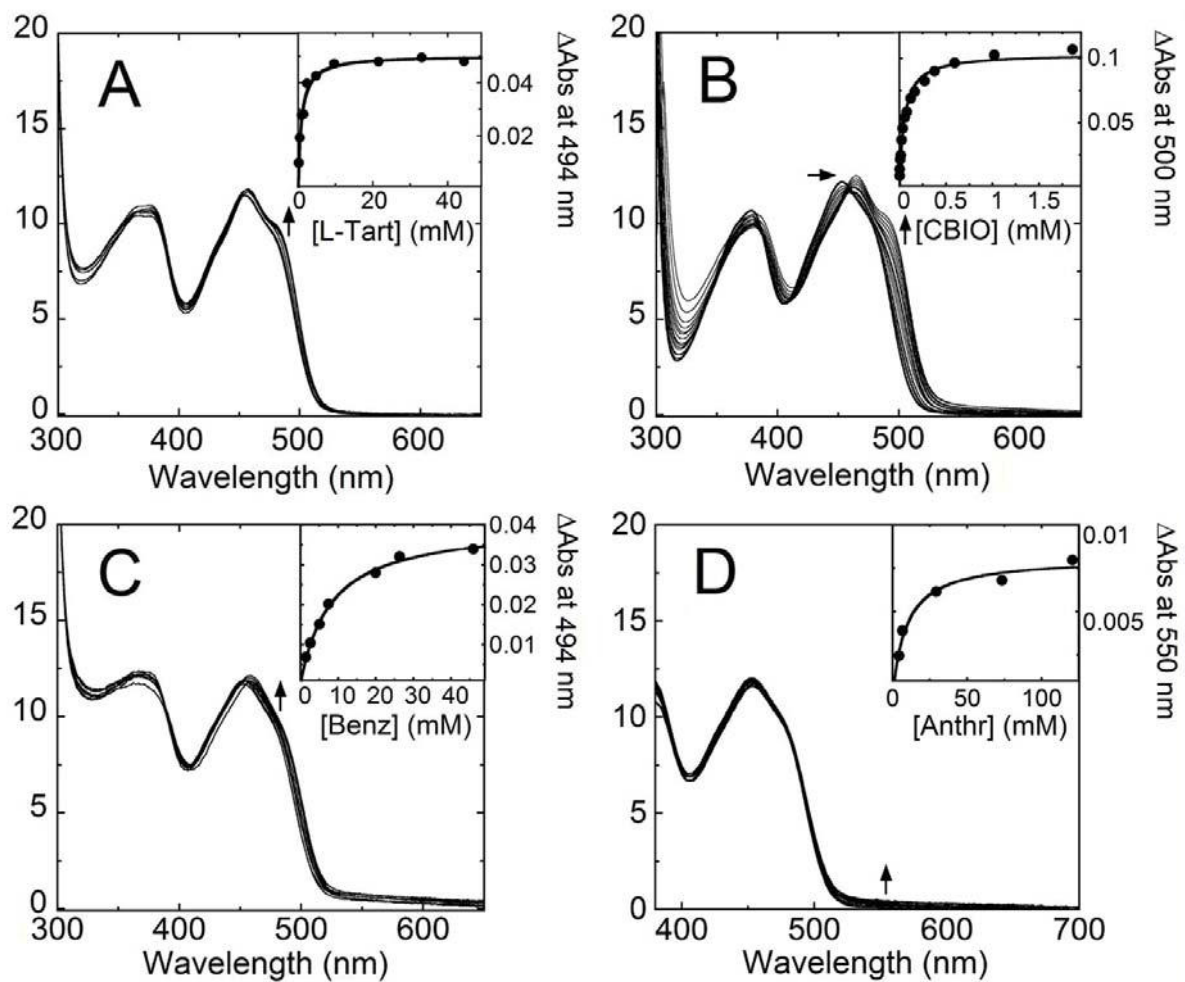
Supplementary Fig. 4. Comparison of CD spectral properties of holo- and apoprotein forms of hDASPO. A) Far-UV CD spectrum (0.1 mg protein/mL). B) Near-UV CD spectrum (0.4 mg protein/mL). Buffer: 20 mM potassium phosphate pH 8.0, 10% (v/v) glycerol; all measurements were performed at 15 °C.



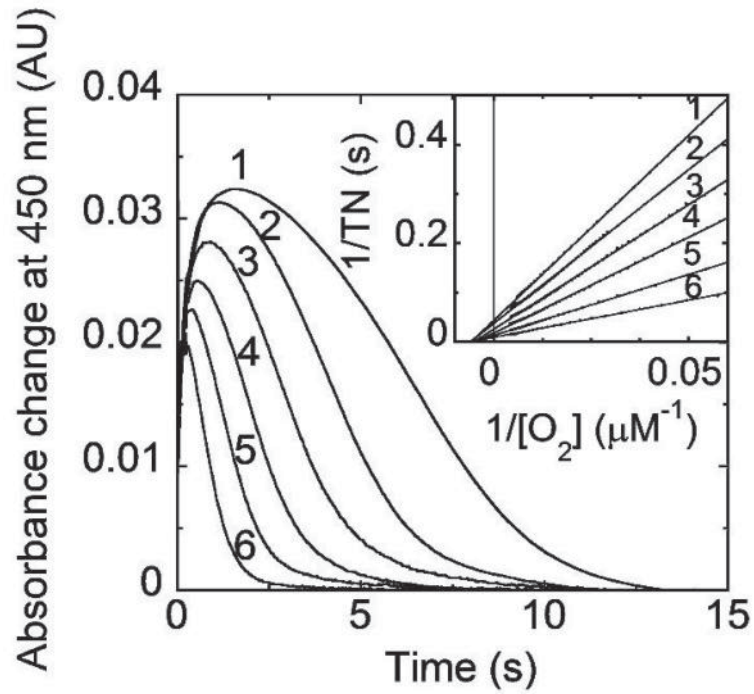
Supplementary Fig. 5. Analysis of thermal denaturation of holo- (----) and apo-(— —) hDASPO obtained following the 220-nm CD signal, in the absence or in the presence of exogenous cofactor and/or ligands (solid lines). A) Denaturation thermal curves of apoprotein and holoenzyme in the absence or in the presence of 60 μ M FAD; B) in the absence or in the presence 0.1 mM 5-An, 1 mM 5-An, 1 mM 5-An and 60 μ M FAD; C) in the absence or in the presence of 8.6 mM meso-tartrate, 8.6 mM L-(+)-tartrate. Enzyme concentration: 0.1 mg/mL. Buffer: 20 mM potassium phosphate pH 8.0, 10% glycerol, 150 mM sodium chloride.



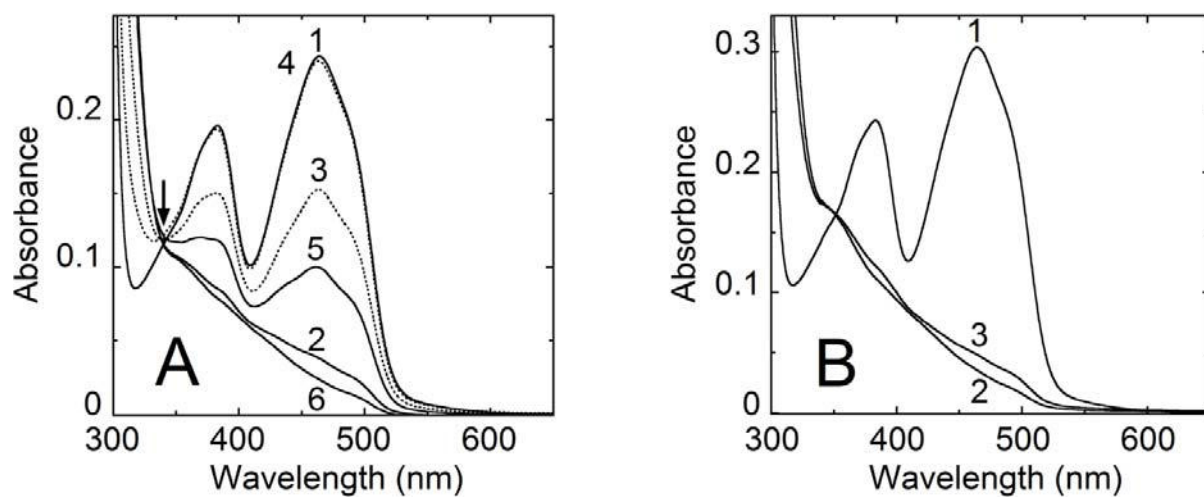
Supplementary Fig. 6. A) Binding of FAD to hDASPO apoprotein in the presence of 40 mM L-(+)-tartrate. Increasing amounts (0-5 μM) of FAD were added to a fixed amount of hDASPO apoprotein (1 μM) and the quenching in protein fluorescence was recorded (excitation wavelength: 280 nm). B) Time course of fluorescence emission at 341 nm during the reconstitution of hDASPO holoenzyme: 0.15 μM hDASPO apoprotein was mixed with 0.75 (black), 1.5 (grey) or 7.5 μM (light grey) FAD. The buffer composition was 100 mM sodium pyrophosphate, pH 8.5, 10% glycerol at 15 $^{\circ}\text{C}$.



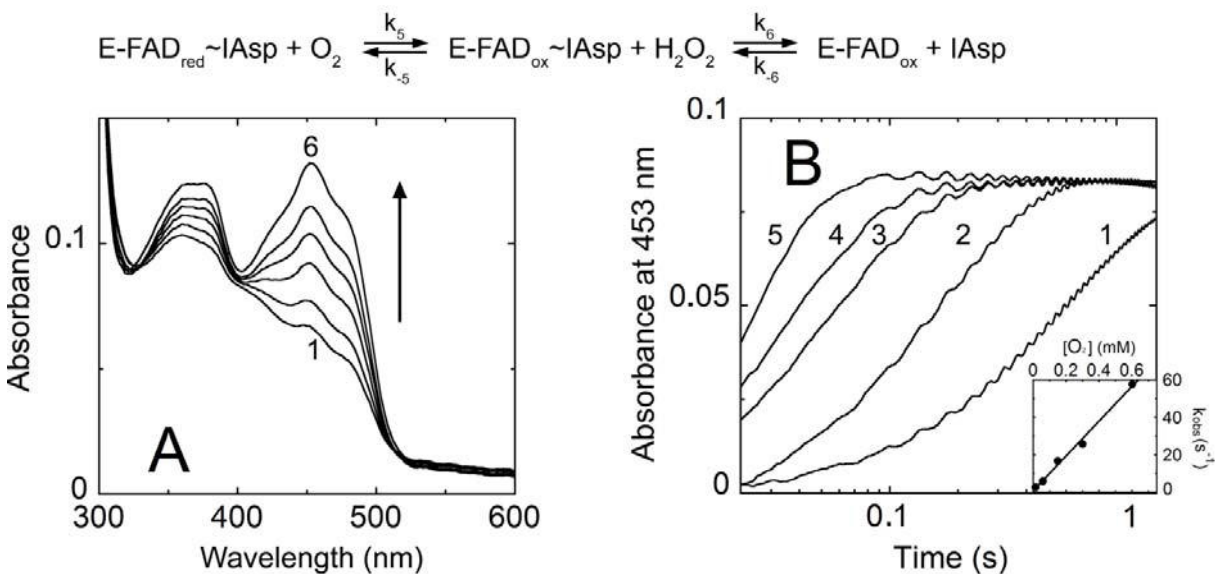
Supplementary Fig. 7. Effect of ligand binding on the visible absorbance spectrum of hDASPO (approx. 12-21 μM). A) L-(+)-tartrate; B) CBIO; C) benzoate; D) 2-aminobenzoate (anthranilate). The latter spectral perturbation is due to the formation of a charge-transfer complex between the ligand and the FAD cofactor: binding affinity is lower compared to tartrate. Selected spectra obtained upon adding increasing concentration of ligands are shown. Inset: fit of the data to a hyperbolic binding curve (solid line). Buffer: 20 mM Tris-HCl and 10% (v/v) glycerol, pH 8.0 at 15 $^{\circ}\text{C}$. Arrows indicate the direction of absorbance change at increasing ligand concentrations. No spectral perturbations were evident up to 40 mM D-(–)-tartrate or 64 mM L-Asp, suggesting that hDASPO does not bind these tartrate and aspartate enantiomers (not shown).



Supplementary Fig. 8. Enzyme monitored turnover of hDASPO on D-Asp in the presence of 0.253 mM oxygen using a stopped-flow spectrophotometer, at 25 °C. The oxidized enzyme, 6.1 μM, was mixed with (1) 0.5 mM, (2) 0.75 mM, (3) 1 mM, (4) 1.5 mM, (5) 2.5 mM and (6) 5 mM D-Asp. The reaction was monitored at 450 nm. Inset: Lineweaver-Burk plot of reciprocal apparent turnover numbers (1/TN) versus the reciprocal [O₂] as obtained by the mathematical elaboration of the data reported in the main panel. Buffer: 100 mM disodium pyrophosphate, pH 8.5, 10% glycerol.



Supplementary Fig. 9. Reversibility of the reductive half-reaction of hDASPO. A) 20.5 μM hDASPO (1) was reduced anaerobically with 28 μM D-Asp in the presence of 8.5 mM ammonium chloride; the reduced enzyme (2) was added of 21 (3) or 38 μM (4) OA (dotted lines). The reoxidized enzyme was newly reduced adding 42 (5) or 124 μM (6) D-Asp. The isosbestic point at 340 nm is indicated by an arrow. B) 24.6 μM hDASPO (1) was reduced anaerobically with 47.6 μM D-Asp in the absence of ammonium chloride (2); the reduced enzyme (2) was then added of 1 mM OA (3).



Supplementary Fig. 10. Oxidative half-reaction of reduced hDASPO-MT complex, at 25 °C. A) Course of reoxidation of 11.9 μM reduced hDASPO in complex with 3.35 mM MT at 25 °C by 12.5% oxygen (final concentrations). The spectra were recorded 20 ms (1), 30 ms (2), 50 ms (3), 70 ms (4), 100 ms (5) and 1 s (6) after mixing. B) Time course of the 453 nm absorbance intensity during the reaction of 10.2 μM reduced hDASPO in complex with 3.35 mM MT at 25 °C, in the presence of 1.25% (1), 5% (2), 12.5% (3), 25% (4) and 50% (5) oxygen (final concentrations). Inset: linear fit of the observed rate constants (k_{obs}) obtained at each oxygen concentration. Buffer: 100 mM disodium pyrophosphate, pH 8.5, 1% glycerol, 2 mM D-Ala, 10 $\mu\text{g}/\mu\text{L}$ catalase, 0.5 μM RgDAAO.